AD_____

Award Number: DAMD17-01-2-0047

TITLE: Disaster Relief and Emergency Medical Services Project
(DREAMS™): Science, Triage and Treatment (STAT)

PRINCIPAL INVESTIGATOR: Samuel Ward Casscells, III, M.D.

CONTRACTING ORGANIZATION: The University of Texas
Health Sciences Center at Houston
Houston, Texas 77030-3900

REPORT DATE: October 2002

TYPE OF REPORT: Annual

PREPARED FOR: U.S. Army Medical Research and Materiel Command
Fort Detrick, Maryland 21702-5012

DISTRIBUTION STATEMENT: Approved for Public Release;
Distribution Unlimited

The views, opinions and/or findings contained in this report are
those of the author(s) and should not be construed as an official
Department of the Army position, policy or decision unless so
designated by other documentation.

REPORT DOCUMENTATION PAGE

Form Approved
OMB No. 074-0188

Public reporting burden for this collection of information is estimated to average 1 hour per response, including the time for reviewing instructions, searching existing data sources, gathering and maintaining the data needed, and completing and reviewing this collection of information. Send comments regarding this burden estimate or any other aspect of this collection of information, including suggestions for reducing this burden to Washington Headquarters Services, Directorate for Information Operations and Reports, 1215 Jefferson Davis Highway, Suite 1204, Arlington, VA 22202-4302, and to the Office of Management and Budget, Paperwork Reduction Project (0704-0188), Washington, DC 20503

1. AGENCY USE ONLY (Leave blank)	2. REPORT DATE October 2002	3. REPORT TYPE AND DATES COVERED Annual (15 Sep 01 – 15 Sep 02)

4. TITLE AND SUBTITLE
Disaster Relief and Emergency Medical Services Project (DREAMS™): Science, Triage and Treatment (STAT)

5. FUNDING NUMBERS
DAMD17-01-2-0047

6. AUTHOR(S):
Samuel Ward Casscells, III, M.D.

7. PERFORMING ORGANIZATION NAME(S) AND ADDRESS(ES)

The University of Texas
Health Sciences Center at Houston
Houston, Texas 77030-3900

E-Mail: S.Ward.Casscells@uth.tmc.edu

8. PERFORMING ORGANIZATION REPORT NUMBER

9. SPONSORING / MONITORING AGENCY NAME(S) AND ADDRESS(ES)

U.S. Army Medical Research and Materiel Command
Fort Detrick, Maryland 21702-5012

10. SPONSORING / MONITORING AGENCY REPORT NUMBER

11. SUPPLEMENTARY NOTES
Original contains color plates: All DTIC reproductions will be in black and white.

12a. DISTRIBUTION / AVAILABILITY STATEMENT
Approved for Public Release; Distribution Unlimited

12b. DISTRIBUTION CODE

13. Abstract (Maximum 200 Words) (abstract should contain no proprietary or confidential information)
Science, Triage, and Treatment is the component of DREAMS (Disaster Relief and Emergency Medical Services) that is developing ways to diagnose and treat tissue injuries and infection. Progress has been the pathophysiology and molecular biology of anthrax, cytochrome P450 defenses, inflammation, oxidation, apoptosis, reperfusion injury, organ failure, and nitric oxide. New techniques have been developed to automatically diagnose ischemia and heart, kidney, and respiratory failure. STAT scientists have also developed techniques to diagnose and image tissue inflammation and necrosis using CT, magnetic resonance, thermal imaging, and near-infrared spectroscopy. These have led to numerous publications, patents, products, clinical trials, and awards. In addition to trauma and infection likely applications include atherosclerosis and cancer. In summary, DREAMS:STAT is making better than expected progress toward the goal of improving the care of battlefield injuries.

14. SUBJECT TERMS:
DREAMS™, disaster relief, triage, treatment

15. NUMBER OF PAGES
85

16. PRICE CODE

17. SECURITY CLASSIFICATION OF REPORT	18. SECURITY CLASSIFICATION OF THIS PAGE	19. SECURITY CLASSIFICATION OF ABSTRACT	20. LIMITATION OF ABSTRACT
Unclassified	Unclassified	Unclassified	Unlimited

NSN 7540-01-280-5500

Standard Form 298 (Rev. 2-89)
Prescribed by ANSI Std. Z39-18
298-102

Table of Contents

Project I.A. "Administrative Section"

Investigator: James T. Willerson, M.D.; S. Ward Casscells, M.D.

We have used these funds to provide administrative support for DREAMS:STAT 2001: secretarial assistance, coordination of the various research programs, statistical analysis assistance and funds for miscellaneous items required by investigators in this project.

All salaries are in accordance with the policies and procedures of the University of Texas-Houston Health Science Center. Fringe benefits are calculated at a rate of 21.5%.

Dr. Ward Casscells is the Principal Investigator for DREAMS:STAT and some financial support for his level of effort is budgeted in this section. Dr. James Willerson is an Associate Principal Investigator and financial support for his level of effort is also included in the budget. Scott Harrison is the Administrator for the DREAMS:STAT program. He coordinates research schedules, administrative reports, purchasing activities, and serves to help each investigator solve administrative problems that arise. Funds are also budgeted for statistical assistance for data evaluation in each of the research sections and for office supplies (including paper, pencils, pens), storage items, computer costs, etc. for each of the investigators.

In general, DREAMS Science, Triage and Treatment exceeded expectations: there were fundamental discoveries as well as practical inventions, mostly in the areas of tissue injury, inflammation, infection, and imaging. Publications, patents, presentations, and awards were numerous. However, the project titled "A Surgical Instrument for Real-Time Analysis" has been replaced by the project titled "Physiological Magnetic Resonance Imaging". After several months of planning and preliminary studies Drs. Willerson and Casscells concluded that the key goals of this project were technically too difficult or expensive, and the other goals were achieved by other teams of investigators.

Several DREAMS 2001 technologies are already being tested in clinical trials, including two types of catheters. The first is a thermography catheter for detection of vulnerable atherosclerotic plaques by the heat they emit, a DREAMS STAT finding that has won several awards and has led to the start-up of at least 4 companies. The University of Texas and the Texas Heart Institute licensed the patents of Drs Casscells, Willerson, and Naghavi to one of these, Volcano Therapeutics. Over 50 patients have already been studied in clinical trials in three countries and European approval is expected in January 2003. The US trial is now underway and FDA approval is expected in late 2003.

The project on hypothermia has also led to new inventions with one patent recently issued and five more being filed. This technology now promises to enable surgeons, pulmonologists, anesthesiolgists, anesthetists, nurses and medics to monitor injured or infected patients or those with heart or lung disease. The catheter is inserted under local or general anesthesia from the internal jugular vein to the apex of the right ventricle where it monitors the bipolar EKG, temperature, pressure, pO2, pH, and pCO2. This is expected to enable automated real-time diagnosis and monitoring of sepsis, myocardial ischemia, heart failure, respiratory failure and renal failure. The technology has led to a device start-up, LifeSentry, Inc.

Of particular relevance to the critical role of the USAMRMC in bioterrorism, DREAMS PI Dr Casscells founded DefenseOfHouston, the citizen group that on September 6,2002 was awarded the Best Practice Award of the US Department of Health and Human Services. Dr Casscells was chosen to serve on several task

4

forces including the Mayor's Advisory Committee to the Medical Strike Team, the Houston Task Force on Terrorism, The University of Texas Homeland Security Committee, the Governor's Council on Health and Bioterrorism, the Pharmacology and Vaccine task force of the Center for Strategic and International Studies in Washington, and the Bush-Cheney Healthcare Advisory Committee.

DREAMS STAT will, in 2003, continue to develop the basic biology and technology needed to improve the care of battlefield injuries. We are honored to be working with US Army.

Project I.B. "Mechanisms of Cardiomyocyte Injury in Shock"

Investigator: L. Maximilian Buja, M.D.

Introduction: Cardiac myocyte cell death is a clinically important consequence of. endotoxin shock. LPS is the major component from the outer bacterial cell wall that leads to profound and diverse effects in mammalian cells, contributing to the release of pro-inflammatory cytokines (interleukin -1 and TNF-alpha) and depression in cardiac function. During the course of our studies in the last year, we have uncovered an innate protective phenotype of the newborn heart against endotoxin-induced cell death. In the adult heart, cardiac *resistance* to endotoxemic injury may occur after exposure to a sublethal dose of LPS. Together, these two observations in adult and neonatal heart suggest that the heart possess the resources for defense against endotoxin-induced cell death. We propose that the pathway by which this occurs is a characteristic of the developing heart and can be primed in the adult cardiac myocyte by de novo expression of protective genes using pharmacological agents. In the prior report we learned that in the neonatal cardiac myocyte, survival genes, and their protein products, are turned on by activation of NFkB signaling in direct response to LPS. We also demonstrated, using an inhibitor of the Akt/ PKB pathway, wortmannin, that this survival pathway was turned on by LPS but did not contribute solely to NFkB signaling and resistance to endotoxin. Finally in the last report, we began exploring the "preconditioning" effects of cyclo-oxygenase-2 (COX-2) where the anti-inflammatory cytokine CydPGJ2 is low in neonatal cardiac myocytes. Low production of PGJ2 (mediated via both COX-1 and COX-2 pathways) obviates the nuclear translocation of NFkB by phosphorylation of IkB alpha and the onset of apoptotic signaling. However, the exogenous dose of PGJ2 required to achieve this effect is in the low mM range, an order of magnitude higher than exogenous production by the myocytes. A second finding emphasizes recent suggestions that TNF-alpha is cardioprotective since PGJ2 abolishes TNF alpha secretion in neonatal myocytes exposed to LPS. Thus, in conclusion, Akt/ PKB pathways do not play a role as an endogenous protective pathway in neonatal heart. Also although neonatal myocytes apparently cannot produce sufficient PGJ2 to generate the "anti-inflammatory" response, the protective consequences may also reflect the *ratios* of inflammatory to anti-inflammatory cytokines.

Recent evidence has led us in a new and exciting direction. Many hypotheses have suggested that the mitochondrial permeability transition (MPT) leads to opening of a pore through which small molecules (< 1.5 Kd) escape and the membrane potential (DY) dissipates. This opening is believed to be associated with the initiation of apoptosis by the release of cytochrome c [1]. Although this is generally believed to be an irreversible pathway, others have proposed that opening of the pore and the accompanying decrease in DY may provide a transient protection from cell injury [2] by (1) inhibiting the accumulation of increased cellular calcium (driven into the matrix by a potential-dependent uniport mechanism) and (2) decreasing the formation of radical oxygen species (ROS) which require a high redox gradient. Others have refuted this notion by simply pointing out that any pore leak of cofactors and substrates cannot reversibly restore cellular function and therefore protect. were amazed, however, to find that mitochondria in myocytes exposed to LPS, lose their membrane potential in a reversible manner (Figure 1). These myocytes exposed to LPS also demonstrate rapid activation of p38 MAPK (Figure 2) and ERK _ (Figure 3). These signals are known to augment the tissue levels of PPAR-g Cofactor 1 (PGC-1) and increase expression of uncoupling proteins (UCP-3) that reversibly produce a proton leak and decrease mitochondrial DY [3]. Therefore, the goal of the next few months is to determine if this protective mechanism is operant in neonatal cells by following UCP3 expression and the temporal relationship with loss of DY and co-localization with the mitochondria in LPS exposed heart myocytes.

6

1   Crompton, M. (1999) Biochem J 341 (Pt 2), 233-49
2   Ichas, F., Jouaville, L. S. and Mazat, J. P. (1997) Cell 89, 1145-53
3   Puigserver, P., Rhee, J., Lin, J., Wu, Z., Yoon, J. C., Zhang, C. Y.,
     Krauss, S., Mootha, V. K., Lowell, B. B. and Spiegelman, B. M. (2001)
     Mol Cell 8, 971-82

FIGURE 1

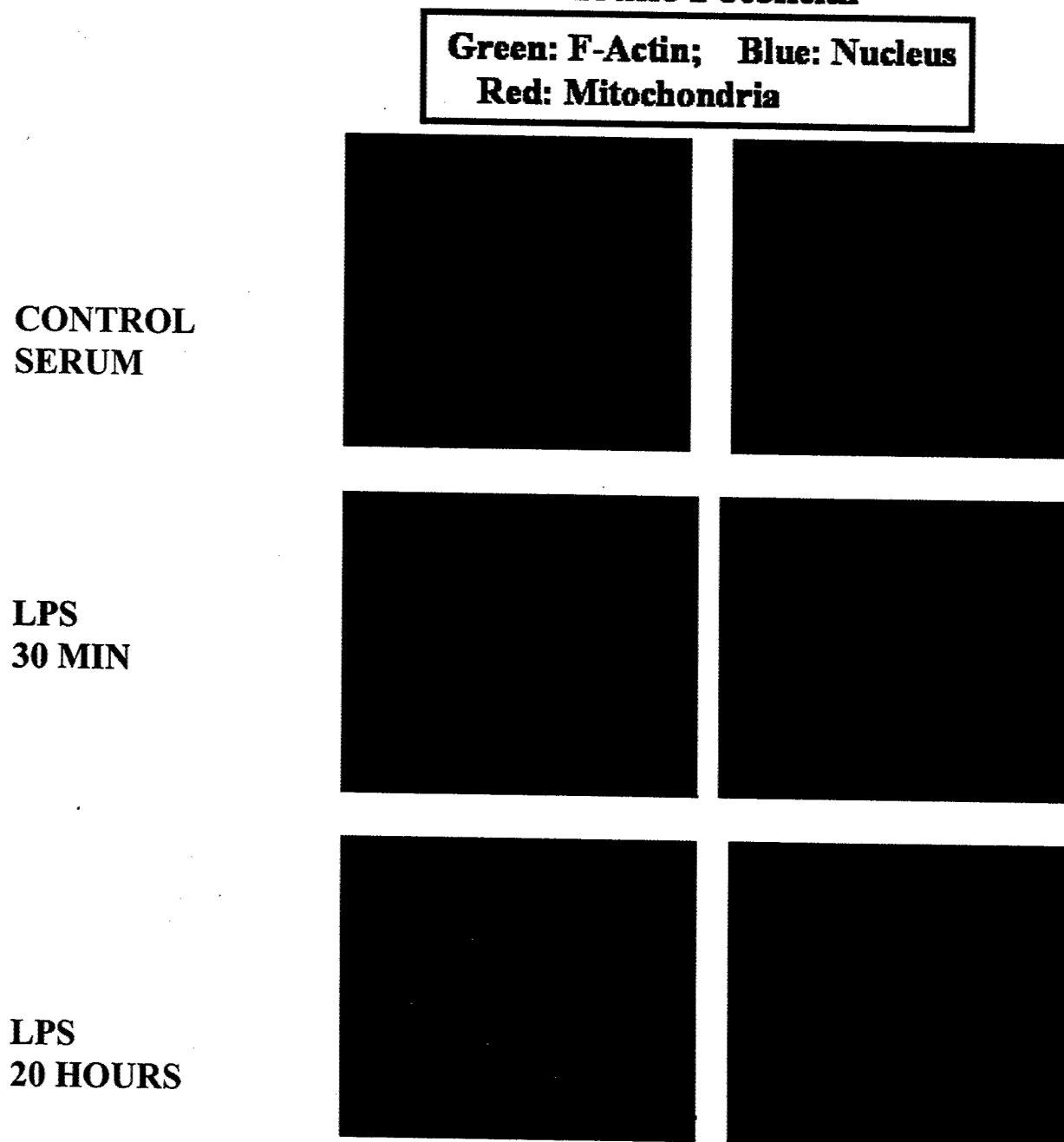# LPS Leads to Reversible Loss of Mitochondrial Membrane Potential

Green: F-Actin;   Blue: Nucleus
Red: Mitochondria

CONTROL
SERUM

LPS
30 MIN

LPS
20 HOURS

Fig. 2

Exposure to LPS Results in Erk Activation

Separation of the phosphorylated bands was achieved using Scion Image Analytical Software.

Fig. 3

Activation of p38 MAPK following Exposure to LPS

P-38 MAPK Whole Protein

Phosphorylated P-38 MAPK

30 Min. to 3 Hours   18 Hours to 24 Hours

Time following Initial Exposure to LPS

Fig. 4

Regulatory Pathway Leading to UCP Synthesis &Mitochondrial Protection

P38-MAPK

LPS

ERK-MAPK   PGC-1

UCP3 Promoter

8

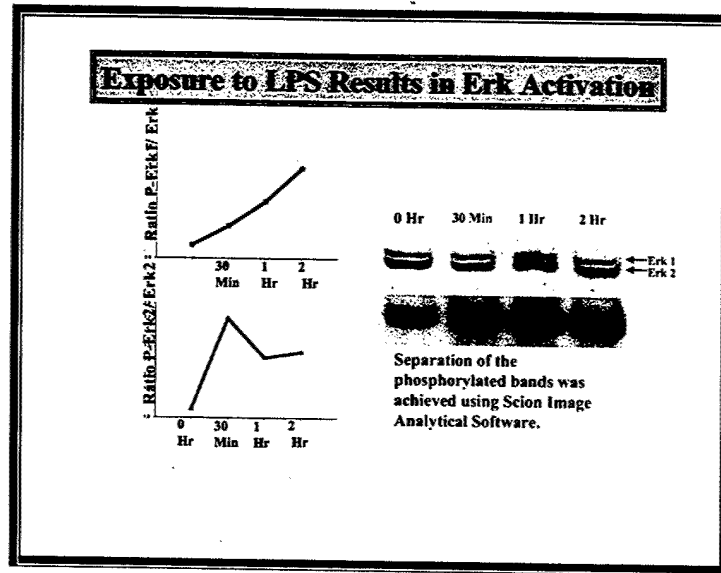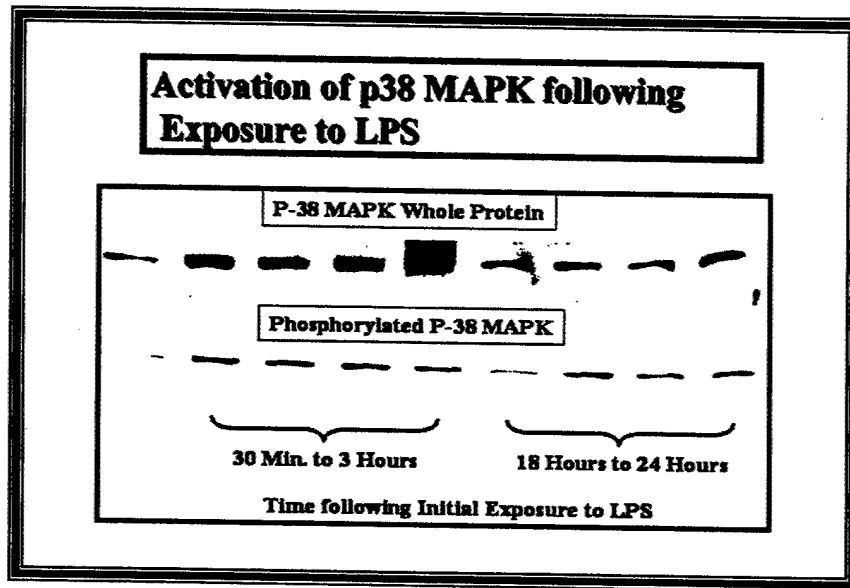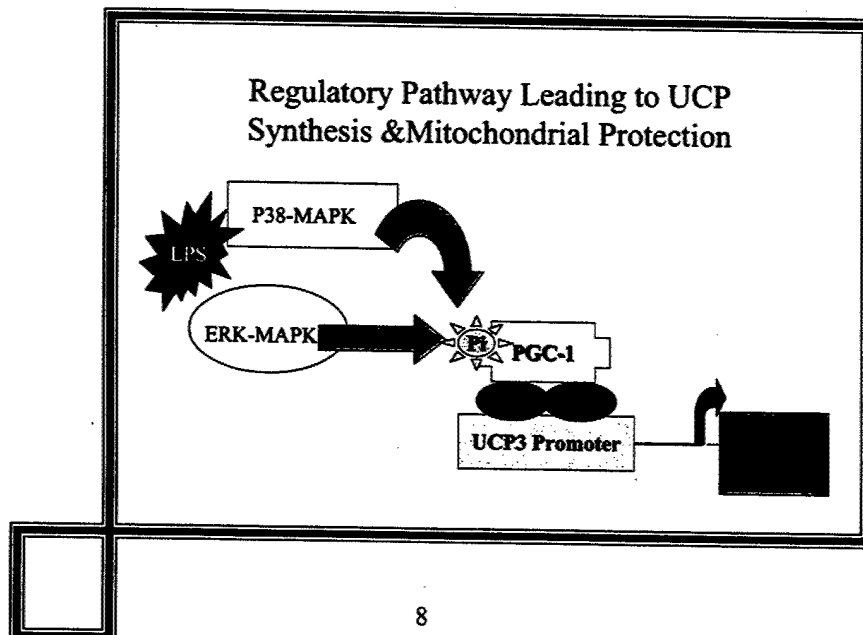**Project IC1: "Molecular Regulation of Apoptosis in Wound Healing"**

Investigator Name: Yong-Jian Geng, MD, PhD

The objectives of the proposed research are to determine molecular mechanisms underlying apoptosis of inflammatory cells and vascular cells during wound healing. In this period, we have focused on the following experiments:

1. Stress proteins and nitric oxide synthesis during the smooth muscle cell response to stress injury by gentle heating.

Inducible nitric oxide synthase (iNOS) responsible for the high output pathway of NO production has been found in atherosclerotic lesions. Proinflammatory cytokines, e.g. interferon gamma (IFN-γ) and tumor necrosis factor alpha (TNF-α), also exist in these lesions and can induce vascular smooth muscle cells (SMC) to express high levels of iNOS. Local induction of iNOS has been implicated in association with vascular damage, apoptosis, and inflammation. On the other hand, the plaque cells express stress proteins, e.g. heat shock proteins (HSPs), in atherosclerosis. In this study we examined whether the stress response by gentle heating affects iNOS expression in SMC induced by inflammatory cytokines. Mouse aortic SMC grown at subconfluence were assigned to either heat therapy or a control group. The cells of stress and control groups were incubated with the DMEM medium with 10% fetal bovine serum at 37°C. The stress group was exposed to the medium pre-warmed and maintained at 42° C for 15 minutes. The control group was treated in the same way except for the temperature setting at 37°C. Two hours after thermal stimulation, SMC were treated with TNF-α (10ng/ml) in the presence or absence of IFN-γ (10ng/ml). After cytokine treatment, nitrite, an end product of NO in the culture media was measured by use of Griess' reagent and total proteins were extracted from SMC for iNOS, HSP and a-actin immunoblotting. Compared to the control cells, cells stressed by thermal stimulation showed a marked reduction in nitrite production (123 ± 50 vs. 73 ± 7.6, $p<0.04$, n=6). Immunoblotting with anti-iNOS demonstrated a reduced intensity of iNOS bands in the stress group. Viability assays with fluorescent dye staining revealed no significant decline in viable cell numbers suggesting that the reduction in iNOS expression was not due to cell death. We further observed that the heat stress markedly induced expression of HSP70, but showed no effect on SM-α-actin expression. Heat shock stress responses enhance expression of HSP70 but inhibit iNOS protein expression and NO

production in vascular SMC triggered by proinflammatory cytokines. The stress responses do not alter cell viability and the expression of cytoskeletal protein, SM-α-actin. These results implicate a novel mechanism by which a moderate stress response such as short-term gentle heating may attenuate an inflammatory reaction by attenuating iNOS expression.

2.   Analysis of cholesterol crystallization in macrophages.

One of hallmarks for atherosclerosis is the formation of cholesterol crystals. Accumulation of the crystals in the arterial wall with atherosclerosis can cause atheroembolism and acute vascular syndrome. Occlusion of the arteries by cholesterol crystals often induces irreversible ischemic damage to the tissue. We examined cholesterol crystals and apoptosis in macrophages (Mφ) in human carotid arteries and apolipoprotein-E deficient (apoE-null) mice, and in phorbol ester-stimulated human THP-1 monocytic cells exposed to different temperatures. DNA labeling and immunohistochemistry revealed that both human carotid and apoE-null aortic plaques contained numerous apoptotic macrophages surrounded by cholesterol crystals. In the "hot" regions rich in inflammatory components such as T cells and monocytes, the crystals were less abundant. Treatment of cultured THP-1 macrophages with 7-ketocholesterol (20 µg/ml), an oxysterol component of oxidized lipoproteins, but not the same amounts of free cholesterol and 25-OH-cholesterol at 37°C for 48 hours, promoted sterol crystal formation. Cell viability assay, in situ detection of DNA fragments, and agarose gel electrophoresis revealed increased apoptosis in the 7-ketocholesterol-treated Mφ (29.6%±6% vs. 5.8±1.4% in controls). Fluorescence microscopy showed the presence of the crystals inside and on the surface of lipid-laden foam cells. Fewer crystals were found in the cells undergoing apoptosis. X-ray diffraction confirmed the presence of 7-ketocholesterol crystalline domains (d space 35.8 A) in the membrane of Mφ incubated with 7-ketocholesterol. When cultured at 40°C for 48 hours, the crystal formation markedly declined by 82% in Mφ, while apoptosis increased by 85% in Mφ. In the absence of the oxysterol, increasing temperature neither affected the cell viability nor changed the membrane crystalline domains. These results suggest that hyperthermia enhances apoptotic effect of the oxysterol, but reduces cholesterol or oxysterol crystal formation, which may in turn influence the plaque stability. We will continue this study by analyzing the chemical components of the

cholesterol crystals and determining the effects of lipid-binding proteins on the formation of cholesterol crystals and apoptosis. We will examine the role for scavenger receptor in regulation of apoptosis.

3. Inflammatory cell apoptosis induced by thermal treatment in atherosclerotic plaques.

Increased cell death by apoptosis and local inflammatory cell infiltration represent major events in advanced atherosclerotic lesions or atheroma. Cytokine expression and activation of the transcription factor NK-kB play an important role in regulation of apoptosis and proliferation in a variety of cell types including vascular cells. **Objectives** of this study were to determine the effects of thermal treatment on (1) apoptosis and cytokine expression in human atherosclerotic plaques and (2) activation of NF-kB in cultured human macrophages. **Methods and Results.** Eleven fresh atherosclerotic plaques collected from human cardotid endarterectomy were incubated in DMEM medium at 37oC or 42oC for 15 min, followed by additional 6 hrs incubation at 37°C . The specimens were immediately divided for immunohistochemistry, electron microscopy, and apoptosis evaluation. In situ labeling of DNA fragments (TUNEL) showed a significant increase in TUNEL+ nuclei. Electron microscopy revealed apoptotic morphological changes in many plaque macrophages, and to a lesser extent smooth muscle cells. Quantitative immunostaining for tumor necrosis factor alpha (TNF) and interleukin-6(IL6) immunostains demonstrated that the heated plaques contained low levels of the cytokines. For NF-kB assays, human THP-1 cells were induced to differentiate into macrophages by phobol esters and then incubated with DMEM at 37°C and 42°C for 15 min followed by 6 hrs incubation at 37C. After incubation, the cells were subjected to gel shift assays with radioactive double stranded oligos encoding sequences for NF-kB and AP-1 binding sites. Gentle thermal treatment markedly reduced NF-kB activation. In contrast, the heat effect on AP-1 appeared moderate. **Conclusions.** Gentle short-term thermal treatment   induces apoptosis in human atherosclerotic lesions, reduces expression of pro-inflammatory cytokines TNF and IL-6,   and inactivates NF-kB. These data suggest that thermal therapy may have potential for treating advanced atherosclerotic lesions by eliminating macrophages by apoptosis and inhibition of NF-kB.

Project I.C.2. "Infrared Spectroscopic Diagnosis of Vulnerable Atherosclerotic Plaque"

Investigator: S. Ward Casscells, M.D.

ABSTRACT

A non-destructive method is investigated for tissue pH and lactate determination in atherosclerotic tissue in-vitro. This method, in the future, may be useful for doctors to investigate the metabolic process of atherosclerosis in-vivo, using an optical catheter-based procedure. In this study, partial least-squares (PLS) is used to develop calibration equations relating visible and near-infrared (NIR) spectra to the tissue pH and lactate concentration in atherosclerotic plaque after surgical removal from diseased carotid arteries. The tissue is heterogeneous and contains variable levels of scattering and absorbing components. Tissue pH is determined from pH-related changes primarily in the hemoglobin (Hb) absorption spectrum. Lactate is determined from known absorbance bands at 2250 and 2295 nm, with a shoulder region at ~2030 nm. PLS models were developed using the full spectral range and optimized range(s). Leave-one-out cross-validation was performed.

RESULTS: Preliminary data suggests tissue pH and lactate determinations are feasible and correlated to the heterogeneous atherosclerotic tissue values in-vitro. Loading vectors for the lactate determination are indicative of the pure component peaks in a six-factor model. CONCLUSIONS: Additional data and model optimization may improve the determinations and the accuracy to clinical needs. The in-vitro data establish the feasibility of an optical, in-vivo catheter-based measurement.

Introduction

The lack of an accurate technique to diagnose vulnerable plaque, or quantitative information that feasibly could aid in the prediction of a sudden cardiac event, that is intuitive, clinically relevant, and

inexpensive, presents a significant medical challenge. The problem has been long outstanding, and requires a novel solution that can deliver both chemical and structural information about the diseased vessels to the physician. The principles of optical spectroscopy, chemometrics, and engineering design, combined with the medical necessity, form the framework for a unique scientific research opportunity to develop an optically based technique. The research would require an understanding of atherosclerotic tissue energetics and tissue optics. The knowledge will aid the development of a clinical instrument for the detection of vulnerable plaque. The contributions to the understanding of the vulnerable plaque should be made clear and evident, and the contrast to other techniques highlighted so that the new method can gain acceptance in the medical community.

The Specific Aims of the Research

The intent of this research is to show the feasibility of using near infrared spectroscopy (NIR) to accurately determine metabolic derangements (namely, tissue pH and lactate concentration) in living human atherosclerotic lesions. This is accomplished through the design of a small, fiber optic-based, reflectance-mode spectroscopic sensor to collect continuous optical spectra (400-2400 nm) from an approximately 1-mm^3 volume of the interior portion of a vessel wall. The custom designed optical sensor is used with *in-vitro* experiments of freshly excised human carotid artery atherosclerotic plaques. The optical spectra will be matched with the reference measurement of the metabolic status of the living plaque. Multivariate mathematical models will be developed, reducing the optical spectra to the most relevant factors that correlate with the individual reference measurements. These models will serve as a calibration of the NIR optical system. The model(s) capability to predict the desired parameter(s) from unknown optical spectra will be tested using accepted techniques for small sample sizes (*N<100*). The performance of the optical probe will be assessed by the calibration accuracy.

13

For the purposes of this research, the optically determined tissue pH and lactate values obtained from the statistically-based, empirical models will be only be reviewed as to its possible correlation to the current destructive method of classifying atherosclerotic lesions and vulnerable plaques identification (i.e. histology). At the conclusion of this phase of research, it is hoped that the *in-vitro* model developed can be translated to an appropriate *in-vivo* animal model validation, with at the very most, minor additional destructive experimentation for improving model accuracy and predictability. It is not the intent of this research study to definitively answer whether optically determined metabolic status based on tissue pH and/or tissue lactate is sensitive and/or specific enough alone to differentiate different atherosclerotic lesion types or vulnerability. Acceptance criteria for the calibration will be drawn. Limitations will be discussed for both the feasibility of using optical spectroscopy and for the long-term objective of making a clinical optical spectroscopy catheter that can predict plaques that are vulnerable to rupture. An additional contribution that this research has--on simply gaining a better understanding of the gross metabolic properties of atherosclerotic lesions--will help future researchers develop better diagnostic and therapeutic agents to reduce the sudden cardiac death mortality, and possibly aid in the prevention of heart attacks.

The short-term goals must first be achieved to realize the potential benefit to society. The following specific aims outline how these research goals will be met:

1) Design a reflectance-based optical fiber probe that uses visible to near-infrared light optimally to interrogate a small volume of tissue. The target of a 1 mm^3 tissue volume is based on the normal wall thickness of a coronary artery, the average thickness of atherosclerotic plaques with less than 70% blockage of the artery, and a plausible x-y plane of heterogeneity with respect to the atherosclerotic plaque.

a) Perform Monte Carlo simulations using optical properties of vessel wall and atherosclerotic lesions described in the literature. Infer possible source-receiver fiber separations that meet target volume.
b) Design and build fiber optic probe(s) using the simulation results as a starting point (*first design iteration*).
c) Collect and analyze 400-2400 nm optical spectra using the fiber probe(s) and their different source-receiver separations on normal and atherosclerotic portions of vessel walls. Estimate signal-to-noise ratio at different key wavelengths and implement design improvements (*second design iteration*).

2) Using the optimized custom-manufactured optical probe built after second design iteration, estimate the depth penetration. Measure the depth penetration at key wavelengths by successively stacking thin sections of non-diseased tissue on to the end of optical probe and collecting the reflectance spectra. Compare to theoretical calculations and estimate resulting tissue volume over the wavelength region studied.

3) Perform *ex-vivo* atherosclerotic plaque studies using the different optical probe designs and develop a preliminary multivariate calibration using partial least-squares methodology.
a) Using two design configurations on carotid plaques *ex-vivo* (side viewing and forward viewing fiber optics), evaluate suitability to the experimental methods, signal obtained, and long-term objectives.
b) Identify major interferents to the optical spectra and reference measurements. Determine which may prove to be significant to the calibration accuracy. Propose or develop methodology to reduce their effects.
c) Develop acceptance criteria to demonstrate feasibility based on preliminary multivariate calibrations.

4) Using optimized fiber optic probe matched to system instrumentation, collect and analyze large calibration set of human carotid endarterectomy specimens (50-100 data points) while maintaining physiological state *in-vitro*.
a) Show that the stability of metabolic parameters over time course of data collection can be achieved using tissue culture techniques. The stability is required to mimic *in-vivo* situations and decrease time-correlated effects on the measurements.
b) Perform multivariate calibration using wavelength selection and/or signal conditioning for NIR tissue pH and tissue lactate determinations.
c) Compare the NIR-predicted values from the empirical model to the reference measurements using calibration metrics of correlation coefficient (R^2), root mean squared deviation (RMSD), and the number of factors needed for model accuracy. Review acceptance criteria and make recommendations.

Hypotheses and Research Methods

Hypotheses

The main hypotheses of this research are:

1) Reflectance optical spectroscopy, using visible to near infrared light energy, can be used *in-vitro* to develop calibration equations that provide an optical determination of the atherosclerotic tissue pH and lactate concentration.

2) A small fiber optic prototype (< 3 mm optical working diameter) will make reliable optical measurements *in-vitro* for the assessment of metabolically active plaque. Both theoretical and practical considerations are allowed for in the design and implementation. The performance will be determined by calibration accuracy.

3) An evaluation of the major unmodeled experimental factors that may affect calibration accuracy can be made. The *in-vitro* temperature, experiment time, and the gross plaque constituent information, are identified *a priori* as important factors that will be compiled and listed. Statistical analysis will be performed to determine the significance of these parameters to the overall performance of the fiber optic prototype.

4) Individual mathematical models can be developed which relates the corresponding optical spectra to the individual metabolic parameters, measured with accepted reference methods, in ~30 different atherosclerotic plaques, in the presence of inherent pathological variability. By collecting the optical spectra in a controlled, stable *in-vitro* environment and by using partial least-squares (PLS) multivariate calibration, accurate determinations will be achieved for the individual metabolic parameters of plaque tissue pH and plaque lactate concentration. The correlation coefficient of the determination and root mean squared deviation will be used to determine calibration accuracy. The number of factors will be used to determine the appropriateness (e.g., overfit/underfit) of the calibration.

Research Methods

Methods and apparatus based on reflectance-mode spectroscopy of visible and near-infrared light energy was chosen to solve the main research problem (Chapter 1) for the following reasons:

- Standard medical-grade optical fibers can provide inexpensive, remote, vascular access to the atherosclerotic lesion or known diseased areas. Optical spectroscopy can provide specific biochemical information, unlike intravascular ultrasound (IVUS), or magnetic resonance (MR) catheters that currently provide only structural information.

- The potential for Catheterization Laboratory research and clinical use is enormous.

- Preliminary results in Dr. Soller's laboratory show tissue pH can be feasibly determined by optical reflectance spectroscopy in several different tissue beds. [29-31] Other researchers have used optical methods to determine lactate and other metabolites in cell culture [32], and blood plasma [33].

- No other researchers have reported results on using this method for determining the metabolic status of atherosclerotic lesions. This is a novel approach based on the idea that vulnerable plaques are more metabolically active than the stable plaque or background vessel wall. This research will contribute significantly to the existing knowledge in the field of vulnerable plaque research.

There is considerable histological and metabolic heterogeneity in human

atherosclerotic lesions. [28,34] Optical spectroscopy is one of the few

techniques available for non-destructive analysis. It is also relatively

inexpensive compared to other modalities such as NMR, B-mode ultrasound, and

nuclear (x-ray) radiography. Near-infrared (NIR) spectroscopy has been proposed by several researchers (Lodder [35], Muller [36], Feld [37], Jaross [38], Wang [39] et al) to characterize the properties of vulnerable atherosclerotic plaques, such as thin cap and large lipid core. However, in this previous body of work they were not able to resolve the issue of the inherent tissue heterogeneity with respect to these histological variables and their optical measurement. The apparent mismatch is identified as a key reason why the optical methods accuracy is less than desired.

Preliminary experiments and calibration model development for tissue pH and lactate are conducted to work out any needed improvements in the collection of optical spectra and the methodology. The potential confounding but unmodeled experimental variables are identified a priori as the in-vitro tissue temperature, the experiment time, and the gross pathology of the atherosclerotic plaque. The thickness and the co-registration of optical spectra to the reference measurement (i.e. tissue pH or lactate) are documented. The existence of other systematic errors that affect the optical determination or the multivariate calibration model development, if any, shall be evaluated as well. The final large-scale in-vitro experiments are conducted in oxygenated tissue culture media with temperature control. The stability of this methodology is validated over time by using a PCO_2, PO_2, and tissue pH multi-parameter sensor for several different plaques. The maximum data collection time is fixed at four (4) hours to ensure tissue stability for all plaque types and thicknesses. The in-vitro experimental stability acceptance criteria are derived directly from the validation of the experimental method (see Chapter 6). Separately, the optical penetration depth is measured and deemed acceptable. The effect of the unmodeled variables will be determined after the first set of calibration models have been developed. The feasibility of the optical determination of plaque

tissue pH and lactate concentration in the context of these unmodeled variables will be assessed.

The optical calibration model development process will begin with a multivariate technique called partial least squares. It is the technique known to work for tissue pH in other applications in Dr. Soller's lab. Different wavelength regions for the tissue pH and lactate determination will be used and selection criteria developed based on model improvements. The calibration model statistics will be reviewed and standard calibration set acceptance criteria (such as the F-ratio for outlier detection and minimum PRESS for optimal number of factors) will be used.

Figure 3.2.1 shows a flowchart for this research approach. The major components are the optical design and experiment development, the *in-vitro* carotid plaque studies, and finally the multivariate calibration model development. The design and experiment process is usually iterative, however, for the purposes of this studies, performance of the second iteration is demonstrated.

The optical design process involves several steps, including:

- Definition of optical probe requirements;
- Theoretical considerations of tissue optical properties;
- Monte Carlo simulations interpretation;
- Building and testing several optical probes;
- Depth penetration assessment

Once the optical probe has been designed and built to address as many of the issues as possible, a large-scale *in-vitro* testing program will provide the data for the optical calibration models. Factors that may influence the results will be documented and/or compensated. If necessary, new requirements or acceptance criteria will be drawn, and the performance

reviewed against the new criteria. The calibration model development is a complex, statistically based empirical process involving, but not limited to, data compression, factor analysis, and outlier selection. The performance of the final optical prototype will be evaluated using standard metrics in the multivariate calibration or chemometrics literature. Finally, the applicability of the prototype's performance towards detection of the vulnerable plaque via metabolic status and recommendations for future modifications to either the optical design or calibration method will be addressed.
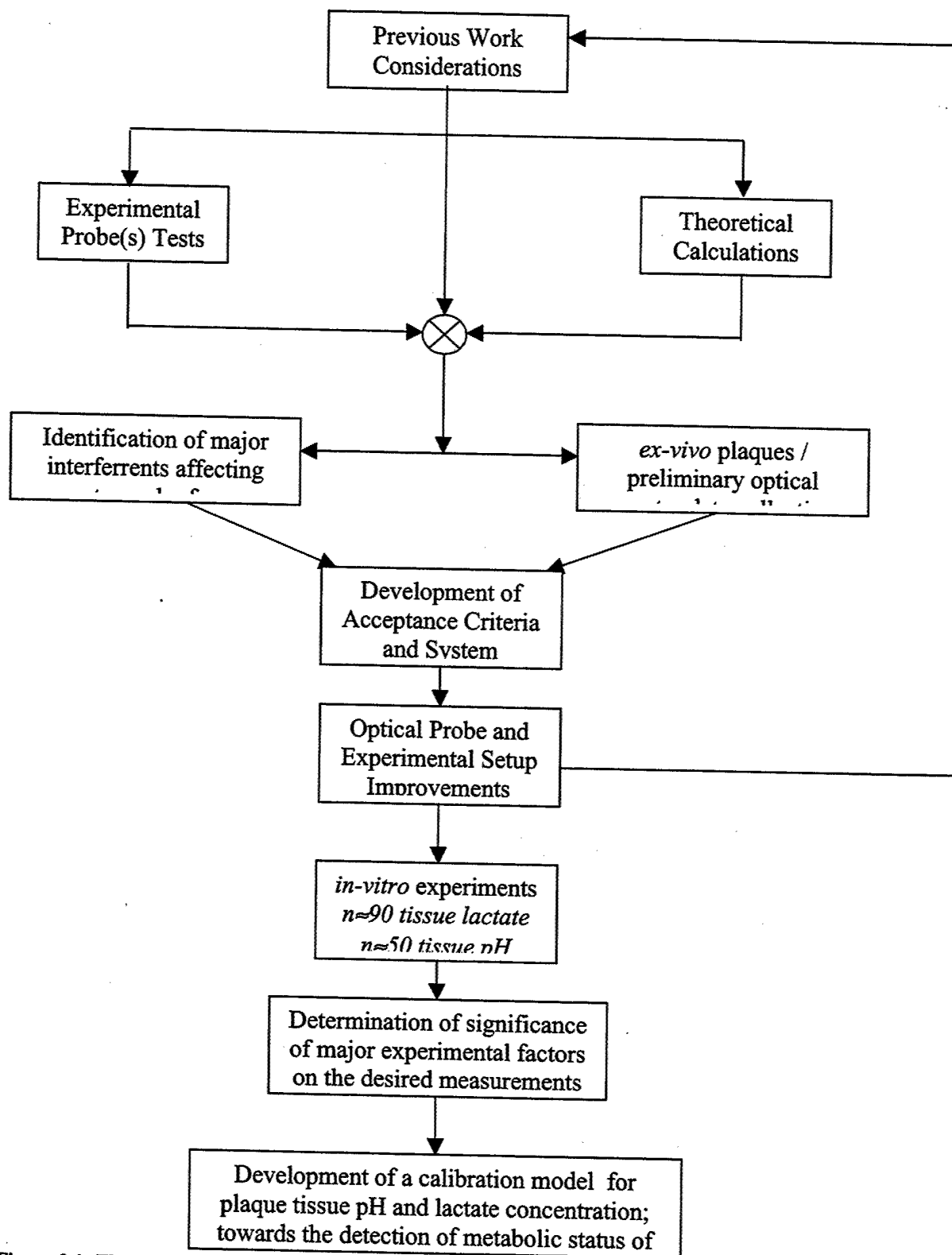
Figure 0.1: Flowchart for research approach.

Background

This research endeavors to establish the feasibility of optical

determinations of metabolic status in the atherosclerotic plaque by using

near-infrared spectroscopy through a small, localized fiber optic probe. Specifically, the plaque tissue pH and tissue lactate concentration are used as the primary indicators of metabolic status in an *in-vitro*, temperature-controlled environment. The methodology described within shall also serve for future spectroscopic catheter validations in hope to bring the near-infrared spectroscopy technique *in-vivo*.

- Atherosclerosis is an arterial disease that has different pathophysiologic outcomes. In the heart, plaque buildup may cause stenosis and/or be thrombogenic (prone to rupture or form clots), leading to sudden cardiac death. The causes of atherosclerosis can be attributed to many risk factors and bloodstream agents. These agents are believed to weaken the endothelial lining of the vessel wall and allow deposits to accumulate and/or further decrease the oxygen tension in the vessel wall. There are many manifestations of atherosclerotic disease in the body, but vulnerable plaque (not angiographically apparent but rupture prone) causes the most damage (or death) when it is in the coronary, carotid and femoral arteries.
- Standard care for high-risk patients include angiographic or ultrasound assessment of stenosed vessel(s), followed by surgery (or catheterization/stenting), and/or pharmocologic therapy (e.g. statins such as Zocor®). Sudden death occurs in the general population from those low to moderate-risk individuals with no previous symptoms (the so-called silent atheroma). Calcium buildup may play important part in stabilizing plaque; a milieu of fat and proteolytic enzymes or acids may change metabolic status of vessel wall.
- Presently, there is no monitoring technique that meets the major requirements of a cost-effective, clinically acceptable, and useful instrument to assess atherosclerotic plaque vulnerability.
- Many investigators have shown that less than 70% stenosis of a vessel does not accurately predict whether one will have a heart attack. Morphological and physiological makeup of the plaque is considered to be more important than % stenosis in predicting dangerous blockages that cause sudden heart attack and/or death.
- Spectroscopic measurement of tissue pH using multivariate calibration techniques is a feasible method for assessing metabolic status of tissue. With advances and understanding of interferents, both experimental and physiological, one can monitor tissue pH and/or lactate concentrations in various tissue beds. The application for atherosclerotic vessel walls is the main focus of this research.
- It is possible to develop a mathematical model relating the optical spectra to the tissue pH or lactate concentration of the atherosclerotic plaque. The experimental factors of temperature, time course, and gross pathology variability are identified *a priori* as possible major variables that degrade the mathematical models and ultimately, the performance of a fiber optic based, near-infrared spectroscopic device.

21

Optical Design

Based on the theoretical simulations, experimental optical tests, and the depth penetration testing, it was concluded that by:

- Using a source-receiver separation of 50 microns provides adequate depth resolution in plaque in both the visible and near-infrared;
- Increasing the collection fiber size to 200/220/240 micron with improved transmission out to 2400 nm improves the signal-to-noise ratio by improving the fiber collection area by 4 times and collection efficiency; and
- Using a 0.5 mm thick quartz optical window fused on the common end, with forward-viewing optics,

a probe could be built that would have adequate resolution for accurate optical determinations in atherosclerotic plaque in a controlled environment with careful registration of the optical and reference measurements. It was expected that *at least* a ~6-fold improvement in the visible region (or an actual voltage of 0.24 mV vs. 0.04 mV) and ~10-fold improvement in the NIR region (or an actual voltage of 130 mV vs. 13 mV) would be realized for the source-receiver separation of 50 microns as compared to the first design iteration probe (Probe #2). The measured improvements were higher, (12-fold improvement in the visible and ~19-fold improvement in the NIR). The practical considerations in the optical design process were able to improve the signal-to-noise ratio, maintain the necessary source-receiver separation, and collect light from a small (<1 mm^3) region of tissue, based on both the experimental and theoretical depth penetration results.

6. Preliminary Experiments, Data Collection, and Analysis

6.1. Optical Spectra

The final probe built and used for the data collection is a slight modification of probe #8. (The original probe #8 was destroyed in the Great Flood of Houston June 9, 2001 where 13 people and 75 monkeys actually died). The current 3 mm outer diameter probe (Remspec, MA) uses a 1.5 m long cable with 200-micron core ultra-low OH fiber. Seven fibers are arranged hexagonally as the input fibers in one leg, and 12 in the other leg to the receiving spectrometer's detector. The center source fibers are separated from the outer 12 fibers by a 50-micron thin walled plastic tube. A 1 mm quartz window (n=1.44) is mounted on the end of the common end. All optical spectra were collected using this probe. The probe is cleaned with an alcohol pad between each tissue spectrum.

6.1.1. FT-NIR Spectrometer

Optical reflectance spectra (1100 – 2500 nm) were taken using a Nicolet Nexus 670 Fourier transform near infrared-based spectrometer with an uncooled InGaAs detector, and converted to absorbance using a 50% reflectance standard (Labsphere, NH). The source is a built-in 75 Watt tungsten lamp and the modulated energy is focused into the fiber optic probe using a lens adapter system provided with the spectrometer. The reference detector voltage was checked for stability after the spectrometer was allowed to warm up for ~ 1 hour (±4.6 volts). The signal off of the 50% reflectance standard was set, using a micromanipulator to adjust the probe height, to provide a center burst interferogram voltage of 0.50/-0.45 V, with auto gain for each

reference intensity measurement. The reference spectrum was measured prior to each tissue spectrum in this manner. This procedure allowed the signal from the fiber optic probe to have the best possible signal-to-noise ratio given the known fiber optic-to-FT spectrometer losses. The resulting spectral resolution is approximately 2.5 nm and the acquisition time is ~42 seconds. These spectra are used for both optical determinations.

6.1.2. Dispersive Spectrometer

Optical reflectance spectra (380 – 1100 nm) were taken using a Control Development (South Bend, IN) 512 element photo-diode array spectrometer with an uncooled Si detector, and converted to absorbance using the same 50% reflectance standard as above. The spectral resolution of the spectrometer is 2 nm. The source is an unmodulated, separate ~7.5 Watt tungsten-halogen lamp (Ocean Optics, FL). After the 50% reflectance standard is measured on the FT spectrometer, the source and receiver fiber optic connectors are removed from the Nicolet FT spectrometer and placed on the Ocean Optics source and Control Development spectrometer respectively. The probe height is maintained and a reference spectrum is taken prior to each tissue spectrum. The maximum reference signal at 727 nm was checked (after the spectrometer and source were allowed to warm up for ~1 hr) to be within ±5% of 45,000 A/D counts (minus the background dark current signal, measured prior to each reference signal). The integration time was set to be 3.6 seconds, and sample averaging to 15, resulting in an acquisition time of 54 seconds. These settings allowed the tissue spectra to be collected at the maximum signal-to-noise ratio possible with the depressive spectrometer in a reasonable time. The tissue spectra are then offset at 970 nm and

24

spliced to the near-infrared spectra collected by the Nicolet. The full range spectra (380-2400 nm) were only available for a subset of the optical determinations.

6.2. Reference Measurements

Co-registration of the location of optical spectra and the reference measurements was made by utilizing a visual mapping grid and a rigid plate tool to fix the plaque specimen within the physiological media dish. First, the plaque was fixed to the plate tool at specific holes corresponding to the map. An outline tracing of the plaque was made on the map matching the holes and dimensions. Plaque features and gross pathology were also observed and noted on the drawing. A digital picture of the plaque on the plate tool was taken for future reference. Second, a random area was chosen for the optical probe to be placed, and registered with a map location such as A1, B1, C1, A2, and so forth. The optical probe was placed in the micromanipulator and allowed to contact the plaque through the liquid media at a constant pressure determined by deflection of weight of the media-dish system. After the optical spectra were taken, the micromanipulator was adjusted back to the original weight, allowing the light to be seen directly under the probe, reflecting off of the plaque location from which the spectra were taken. Next, a T-type needle thermistor probe was placed into the tissue directly under the optical probe and the tissue temperature recorded. The tissue micro-pH electrode was then carefully inserted in the same location as the needle thermistor probe at a depth of ~0.75 to 1 mm into the tissue and recorded. Lastly, the 4-mm diameter biopsy device was then placed at ~45° angle to the optical probe and allowed to cut into the plaque at the junction. The optical probe was removed, and the tissue biopsy was taken of the area just under the optical

25

probe. Extreme care was taken to make sure the area biopsied was the same as the map location and through the entire thickness of the plaque. The thickness of the biopsy itself was measured and ~1/2 to 2/3 from the center of the biopsy was snap frozen in liquid nitrogen; the rest was placed in a histology cartridge for processing. Each biopsy was labeled with the map location. Lastly, all tissue spectra are reviewed to see if the rigid plate tool is inadvertently reflected in the signal, by collecting a media/plate spectrum (without plaque). The apparatus for the specific reference measurements of tissue pH and tissue lactate are summarized below.

6.2.1. Tissue pH

Micro-pH electrodes in a sharp, beveled 21-gauge needle (~750 um diameter, MI-407 Microelectrodes Inc., NH) were used to make the reference plaque tissue pH measurements with the reference junction electrode placed in the media. The beveled needle allowed for quick and easy penetration into the fibrous and calcified plaques. The electrodes were calibrated prior to each plaque experiment using a Thermo Orion 720A pH meter and five NIST-traceable buffers (Fisher Scientific, 4.00, 6.00, 7.00, 7.40, and 10.00 at 25°C). The calibration slope was recorded each day. The tissue readings were recorded at the precise map locations when the pH meter reading was stable. The pH measurement was automatically temperature corrected to the *in-vitro* media temperature. After each tissue measurement, the electrodes were rinsed in warm Tergazyme solution, then distilled water, checked in 4.00 buffer at 37°C, to avoid protein buildup and electrode drift from location to location. These values were used for the optical calibration of tissue pH.

6.2.2. Tissue Lactate

To obtain reference lactate concentrations for the optical calibration, biopsy samples were immediately collected after the tissue pH and temperature measurements. A 4 mm punch biopsy of the area directly under the optical probe was used, and was registered on drawing grid as described above. Each biopsy piece was placed in a cryovial and immediately frozen in liquid nitrogen. All samples were stored in liquid nitrogen tanks until ready to extract (no more than 6 weeks). Tissue weights were obtained prior to assay using a Sartorius analytical balance. A standard Sigma Blood Lactate Kit UV-340A (Sigma Diagnostics, MO) was adapted to tissue extracts and microplate assay. Tissue extracts were prepared by homogenization according to Lowry and Bergmeyer [89,92]. The neutralized perchloric acid (PCA) tissue extracts and assay reagents were incubated together for 30 minutes at 25°C. The absorbance at 340 nm was read and recorded on a Dynatech Lab MRX Microplate Reader. Calibration curves were generated for each batch run by plotting blank-corrected absorbance vs. concentration (mg/ml) of freshly prepared standards. A percent recovery factor (see below) is calculated and multiplied to the values obtained from the curve. Finally, to obtain a weight basis, the concentration is volume-corrected and divided by the weight of each sample to obtain units of micromoles lactate per gram of tissue. These values are used for the optical calibration.

Percent Recovery Procedure (adapted from Bergmeyer et al [92])

27

In the homogenization and assay process, some tissue is inevitably lost. This loss represents a loss of information that may degrade the optical determination of lactate, due to inaccuracies in the reference measurement. Therefore, for each batch assay, including a percent recovery procedure made an assessment of precisely how much lactate was lost.

One sample was randomly taken and split in half during homogenization step. A known amount of lactate standard (50 ul of 0.4 mg/ml or 0.02 mg lactate) was added to the second aliquot of the sample. The dilution factors were calculated for both the undoped and doped test tubes. Both test tubes were processed as normal through rest of the procedure. To calculate the percent recovery, first the concentration of both samples was determined from the calibration curve. The percent recovery factor is then calculated by assuming what is in the un-doped homogenate is in the second tube plus the value Y as above. That is, if X represents the concentration of lactate in the original homogenate, then X+Y should be the concentration of the doped sample (volume dilution factors accounted). The ratio of the doped sample concentration from the calibration curve and the expected X+Y concentration is the percent of lactate that can be feasibly recovered. This correction is applied to all other samples.

SAMPLE CALCULATION:

Calibration Slope=7.5 Abs. Units/mg/ml lactate   MW of lactate = 90 grams/mole

Calibration Intercept=0.015 Abs. Units

Blank-corrected Absorbance of sample 1 = 0.52

Lactate concentration = (0.52-0.015) ÷ 7.5 = 0.0673 mg/ml lactate or 748 nanomoles/ml

To account for volume added to tissue homogenate in step 1, multiply by supernatant volume correction factor (ex. (200 ul PCA + 20 ul $KHCO_3$)/200 ul PCA). Also account for % Recovery.

To get weight basis, divide concentration by weight of tissue per ml of PCA. For example, if the tissue weighted 15 mg, the above lactate concentration would be reported as:

In this example let % recovery = 85% and amount $KHCO_3$ (neutralization base) added was 20 ul:

748 nanomoles/ml * 1.1 ÷ 0.85 ÷ (15 mg / 0.2 ml)= 12.9 nanomoles/mg tissue or 12.9 umoles /gram tissue.

6.3.   Data Analysis

Galactic Grams/32 software (Galactic Industries Corp., NH) was used to process the optical spectra. The PLS/IQ module was used to perform multivariate calibrations. The reference measurements, biopsy thickness, and observed gross pathology were entered into a Microsoft Excel spreadsheet for each point. Correlations were drawn for tissue pH versus temperature, pH versus lactate, lactate versus temperature, and pH or lactate versus gross pathology. The experimental variables of in-vitro temperature, experiment time, and gross pathology were also entered into Statistica (StatSoft, OK) for statistical analysis with respect to the chronological tissue pH and lactate reference values.

6.4. Summary

The final plaque data collection was performed in an oxygenated MEM, physiological media-dish system at 37°C in a warmed and humidified incubator. The overall experiment time and methodology is validated up to 4 hours. The data collection is performed as such:

- Co-registration and plaque mapping is performed on a grid matching the rigid plate tool to which the plaque is fixed. Locations are picked randomly and the gross pathology is recorded.
- Optical absorbance spectra are collected on two spectrometers from 380 -2400 nm using an optimized, 3 mm diameter optical probe. A constant pressure contact is achieved between the optical probe and plaque tissue.
- Temperature measurement is made in the plaque tissue directly under the optical probe.
- Tissue pH measurement is made in the same location.
- Tissue biopsy for lactate and histology is made in the same location. The tissue biopsy thickness is measured.
- The optical probe and pH electrodes are cleaned prior to moving to the next location.

This procedure is repeated for as many points allowed in the 4-hour time period. The tissue biopsies are stored in liquid nitrogen and batch processed for assay within 6 weeks. The histology is processed

for future reference. Tissue spectra that do not show evidence of the rigid plate tool being reflected are used for the optical determinations. This data collection method is a realistic, *in-vitro* approach. It is hoped that the results could possibly be translated to an *in-vivo* optical determination validation in future work.

Reference List

1. American Heart Association. 2002 Heart and Stroke Statistical Update. 2001.

2. Naghavi M, Madjid M, Khan M, Mohammadi R, Willerson JT, Casscells W. New developments in the detection of vulnerable plaque. Curr Atheroscler Rep 2001 Mar 3;2(3):125-35.

3. Fayad Z, Fuster V. Clinical imaging of the high-risk or vulnerable atherosclerotic plaque. Circ Research 2001;89:305-16.

4. Stefanadis C, Diamantopoulos L, Vlachopoulos C, Tsiamis E, Dernellis J, Toutouzas K, Stefanadi E, Toutouzas P. Thermal heterogeneity within human atherosclerotic coronary arteries detected in vivo: a new method of detection by application of a special thermography catheter. Circulation 1999;99:1965-71.

5. Lederman R, Raylman R, Fisher S, Kison P, San H, Nabel E, Wahl R. Detection of atherosclerosis using a novel positron-sensitive probe and 18-fluorodeoxyglucose (FDG). Nucl Med Commun. 2001;22:747-53.

6. Vallabhajosula S, Fuster V. Atherosclerosis: imaging techniques and the evolving role of nuclear medicine. J Nucl Med 1997;38:1788-96.

7. Ciavolella M, Tavolaro R, Taurino M, Di Loreto M, Greco C, Sbarigia E, Casini A, Speziale F, Scopinaro F. Immunoscintigraphy of atherosclerotic uncomplicated lesions in vivo with a monoclonal antibody against D-dimers of insoluble fibrin. Atherosclerosis 1999;143:171-5.

8. Krinsky G, Freedberg R, Lee V, Rockman C, Tunick P. Innominate artery atheroma: a lesion seen with gadolinium-enhanced MR angiography and often missed by transesophageal echocardiography. Clin Imaging 2001;25:251-7.

9. Bonk R, Schmiedl U, Yuan C, Nelson J, Black C, Ladd D. Time-of-flight MR angiography with Gd-DTPA hexamethylene diamine co-polymer blood pool contrast agent: comparison of enhanced MRA and conventional angiography for arterial stenosis induced in rabbits. J Magn Reson Imaging 2000;11:638-46.

10. Patwari P, Weissman N, Boppart S, Jesser C, Stamper D, Fujimoto J, Brezinski M. Assessment of coronary plaque with optical coherence tomography and high-frequency ultrasound. Am J Cardiol. 2000;85:641-4.

11. Nissen S, Yock P. Intravascular ultrasound: novel pathophysiological insights and current clinical applications. Circulation 2001;103:604-16.

12. Takano M, Mizuno K, Okamatsu K, Yokoyama S, Ohba T, Sakai S. Mechanical and structural characteristics of vulnerable plaques: analysis by coronary angioscopy and intravascular ultrasound. J Am Coll Cardiol 2001;38:99-104.

13. Cassis LA, Lodder RA. Near-IR imaging of atheromas in living tissue. Anal Chem 1993;65:1247-56.

14. de Korte C, Cespedes E, van der Steen A, Pasterkamp G, Bom N. Intravascular ultrasound elastography: assessment and imaging of elastic properties of diseased arteries and vulnerable plaque. Eur J Ultrasound 1998;7:219-24.

15. Jeremias A, Kolz M, Ikonen T, Gummert J, Oshima A, Hayase M, Honda Y, Komiyama N, Berry G, Morris R, and others. Feasibility of in vivo intravascular ultrasound tissue characterization in the detection of early vascular transplant rejection. Circulation 1999;100:2127-30.

16. Uchida Y, Nakamura F, Tomaru T, Morita T, Oshima T, Sasaki T, Morizuki S, Hirose J. Prediction of acute coronary syndromes by percutaneous coronary angioscopy in patients with stable angina. Am Heart J. 1995;130:195-203.

17. Flacke S, Fischer S, Scott M, Fuhrhop R, Allen J, McLean M, Winter P, Sicard G, Gaffney P, Wickline S, and others. Novel MRI contrast agent for molecular imaging of fibrin: implications for detecting vulnerable plaques. Circulation 2001;104:1280-5.

18. Rumberger J. Tomographic (plaque) imaging: state of the art. Am J Cardiol. 2001;88:66E-9E.

19. Achenbach S, Ropers D, Regenfus M, Pohle K, Giesler T, Moshage W, Daniel W. Non-invasive coronary angiography by magnetic resonance imaging, electron-beam computed tomography, and multislice computed tomography. Am J Cardiol. 2001;88:70E-3E.

20. Lehmann K, van Suylen R, Stibbe J, Slager C, Oomen J, Maas A, di Mario C, deFeyter P, Serruys P. Composition of human thrombus assessed by quantitative colorimetric angioscopic analysis. Circulation 1997;96:3030-41.

21. Fuster V, Cornhill JF, Dinsmore RE, Fallon JT, Insull W, Libby P, Nissen S, Rosenfeld M, Wagner W. The Vulnerable Atherosclerotic Plaque: Understanding, Identification, and

Modification. [Anonymous]New York: Futura Publishing Company, Inc.; 1999. 1 p.

22. Stary, H. C., Chandler, A. B., Dinsmore, R. E., Fuster, V., Glagov, S., Insull, W., Rosenfeld, M., dam, Wagner, W., and Wissler, R. W. A Definition of Advanced Types of Atherosclerotic Lesions and a Histological Classification of Atherosclerosis. American Heart Association . 2000. (GENERIC)
Ref Type: Electronic Citation

23. Schoen F, Cotran R. Blood Vessels. In: Cotran R, Kumar V, Collins T, editors. Robbins' Pathologic Basis of Disease. 6 ed. Philadelphia: W.B. Saunders Company; 1999. p 493-541.

24. Schwenke D, Carew T. Initiation of atherosclerotic lesions in cholesterol-fed rabbits. I. Focal increases in arterial LDL concentration precede development of fatty streak lesions. Atherosclerosis 1989;9(6):895-907.

25. Schwenke D, Carew T. Initiation of atherosclerotic lesions in cholesterol-fed rabbits. II. Selective retention of LDL vs. selective increases in LDL permeability in susceptible sites of arteries. Atherosclerosis 1989;9(6):908-18.

26. Williams K, Tabas I. The response-to-retention hypothesis of early atherogenesis. Arterioscler Thromb Vasc Biol 1995;15(5):551-61.

27. Brennan JF, Romer TJ, Lees RS, Tercyak AM, Kramer JR, Feld MS, Adamson AW. Determination of Human Coronary Artery Composition by Raman Spectroscopy. Circulation 1997;96:99-105.

28. Virmani R, Kolodgie FD, Burke AP, Farb A, Schwartz SM. Lessons From Sudden Coronary Death : A Comprehensive Morphological Classification Scheme for Atherosclerotic Lesions. Arteriosclerosis, Thrombosis, and Vascular Biology 2000 May 1;20(5):1262-75.

29. [Anonymous]In-vivo measurement of tissue pH to assess bowel ischemia and reperfusion during hemorrhagic shock. TOPS 1998 Biomedical Optical Spectroscopy and Diagnostics: 1998.

30. Zhang S, Soller BR. In-vivo determination of myocardial pH during regional ischemia using near-infrared spectroscopy. SPIE 1998;3257:110-7.

31. Zhang S, Soller BR, Micheels R. Partial Least-Squares modeling of near infrared reflectance data for noninvasive in-vivo determination of deep tissue pH. Applied Spectroscopy 1998;52(3):400-6.

32. McShane MJ, Cote GL. Near infrared spectroscopy for determination of glucose, lactate, and ammonia in cell culture media. Applied Spectroscopy 1998;52(8):1073-8.

33. LaFrance D, Lands LC, Hornby L, Burns DH. Near-infrared spectroscopic measurement of lactate in human plasma. Applied Spectroscopy 2000;54(2):300-3.

34. Naghavi M, John R, Nakatani S, Siadaty S, Grasu R, Kurian KC, van Winkle B, Soller BR, Litovsky S, Madjid M, and others. pH heterogeneity of human and rabbit atherosclerotic plaques; a new insight into detection of vulnerable plaque. Atherosclerosis 2002;164:27-35.

35. Cassis LA, Lodder RA. Near-IR Imaging of Atheromas in Living Arterial Tissue. Anal Chem 1993;65:1247-56.

36. Moreno, P. R., Lodder, R. A., Purushothaman, I. K., Vyalkov, V., O'Connor, W. N., and Muller, J. E. Characterization of Composition and Vulnerability of Atherosclerotic Plaques by Near-Infrared Spectroscopy. 1999. (GENERIC)
Ref Type: Generic

37. Hanlon EB, Manoharan R, Koo TW, Shafer KE, Motz JT, Fitzmaurice M, Kramer JR, Itzkan I, Dasari RR, Feld MS. Prospects for in-vivo Raman spectroscopy. Phys.Med.Biol. 2000 Feb;45(2):R1-59.

38. Jaross W, Neumeister V, Lattke P, Schuh D. Determination of cholesterol in atherosclerotic plaques using near infrared diffuse reflectance spectroscopy. Atherosclerosis 1999;147:327-37.

39. Wang J, Geng YJ, Guo B, Klima T, Lal BN, Willerson JT, Casscells W. Near-infrared spectroscopic characterization of human advanced atherosclerotic plaques. Journal of the American College of Cardiology 2002 Apr 17;39(8):1305-13.

40. Berne RM, Levy MN. Principles of Physiology. 2nd ed. [Anonymous]Boston: Mosby; 1996. 1 p.

41. Gray H. Gray's Anatomy. 38 ed. [Anonymous]Philadelphia: W.B. Saunders Co; 1980.

42. Yutani C, Imakita M, Ishibashi-Ueda H, Tsukamoto Y, Nishida N, Ikeda Y. Coronary atherosclerosis and interventions: Pathological sequences and restenosis. Pathology International 1999;49:273-90.

43. Levin M. Energy metabolic failure within the arterial wall in atherosclerosis [monograph]. Göteborg University; 2001; 1 p. personal.

44. Libby P. Atherosclerosis: the new view. Scientific American 2002 May;47-55.

45. Manoharan R, Baraga JJ, Rava RP, Dasari RR, Fitzmaurice M, Feld MS. Biochemical analysis and mapping of atherosclerotic human artery using FT-IR microspectroscopy. Atherosclerosis 1993;103:181-93.

46. Moreno, P. R., Lodder, R. A., Purushothaman, I. K., Vyalkov, V., O'Connor, W. N., and Muller, J. E. Characterization of Composition and Vulnerability of Atherosclerotic Plaques by Near-Infrared Spectroscopy. 1999. (GENERIC)
Ref Type: Generic

47. Romer TJ, Brennan JF, Puppels GJ, Zwinderman AH, van Duinen SG, van der Laarse A, van der Steen AFW, Bom NA, Bruschke AVG, Adamson AW. Intravascular Ultrasound Combined with Raman Spectroscopy to Localize and Quantify Cholesterol and Calcium Salts in Atherosclerotic Coronary Arteries. Arterioscler Thromb Vasc Biol 2000;20:478-83.

48. Fuster V, Cornhill JF, Dinsmore RE, Fallon JT, Insull W, Libby P, Nissen S, Rosenfeld M, Wagner W. The Vulnerable Atherosclerotic Plaque: Understanding, Identification, and Modification. [Anonymous]New York: Futura Publishing Company, Inc.; 1999. 1 p.

49. Casscells W, Hathorn B, David M, Krabach T, Vaughn WK, McAllister HA, Bearman G, Willerson JT. Thermal detection of cellular infiltrates in living atherosclerotic plaques: possible implications for plaque rupture and thrombosis. Lancet 1996;347:1447-9.

50. Zemplenyi T, Fronek K. Chemical sympathectomy by 6-hydroxydopamine and arterial enzymes and lactate in the rabbit. Exp Mol Path 1981;34:123-30.

51. Zemplenyi T. Metabolic intermediates, enzymes and lysosomal activity in aortas of spontaneously hypertensive rats. Atherosclerosis 1977;28:233-46.

52. Zemplenyi T, Tidwell DF, Fronek K. Aortic enzymes and lactate in high altitude-raised and cholesterol-fed rabbits. Atherosclerosis 1984;52:233-42.

53. Grasu R, Kurian KC, van Winkle B, Snuggs MB, Siadaty S, John R, Naghavi M, Willerson JT, Casscells W. pH heterogeneity of human and rabbit atherosclerotic plaques [Abstract]. In: Circulation 1999;I-542-I-542

54. Kirk JE. Lactic Dehydrogenase. In: Kirk JE, editor. Enzymes of the Arterial Wall. New York: Academic Press; 1969. p 21-9.

55. Voet D, Voet JG. Glycolysis. In: Voet D, Voet JG, editors. Biochemistry. 2nd ed. New York: John Wiley & Sons; 1995. p 443-83.

56. Romer TJ, Brennan JF, Fitzmaurice M, Feldstein ML, Deinum G, Myles JL, Kramer JR, Lees RS, Feld MS. Histopathology of Human Coronary Atherosclerosis by Quantifying Its Chemical Composition with Raman Spectroscopy. Circulation 1998;97:878-85.

57. Bigio IJ, Mourant JR. Ultraviolet and visible spectroscopies for tissue diagnostics: fluorescence spectroscopy and elastic-scattering spectroscopy. Phys.Med.Biol. 1997;42:803-14.

58. Mourant JR, Johnson TM, Los G, Bigio IJ. Non-invasive measurement of chemotherapy drug concentrations in tissue: preliminary demonstrations of in vivo measurements. Phys.Med.Biol. 1999;44:1397-417.

59. Jaross W, Neumeister V, Lattke P, Schuh D. Determination of cholesterol in atherosclerotic plaques using near infrared diffuse reflectance spectroscopy. Atherosclerosis 1999;147:327-37.

60. Cassis LA, Lodder RA. Near-IR Imaging of Atheromas in Living Arterial Tissue. Anal Chem 1993;65:1247-56.

61. Brennan JF, Romer TJ, Lees RS, Tercyak AM, Kramer JR, Feld MS, Adamson AW. Determination of Human Coronary Artery Composition by Raman Spectroscopy. Circulation 1997;96:99-105.

62. Christov A, Dai E, Drangova M, Liu L, Abela G, Nash P, McFadden G, Maas A. Optical detection of triggered atherosclerotic plaque disruption by fluorescence emission analysis. Photochem Photobiol 2000;72:242-52.

63. Spokojny A, Serur J, Skillman J, Spears J. Uptake of hematoporphyrin derivative by atheromatous plaques: studies in human in vitro and rabbit in vivo. J Am Coll Cardiol 1986;8:1387-92.

64. Soller BR, Micheels R, Coen J, Parikh B, Chu L, Hsi C. Feasibility of non-invasive measurement of tissue pH using near infrared reflectance spectroscopy. Journal of Clinical Monitoring 1996;12:387-95.

65. Hicks GL, Hill A, DeWeese JA. Monitoring of midmyocardial and subendocardial pH in normal and ischemic ventricles. J.Thorac.Cardiovasc.Surg 1976;72(1):52-6.

66. Warner KG, Khuri SF, Marston W, Sharma S, Butler MD, Assousa SN, Saad AJ, Siouffi SY, Lavin PT. Significance of the transmural diminution in regional hydrogen ion production after repeated coronary artery occlusions. Circulation Research 1989;64:616-28.

67. Kumar G, Schmitt JM. Optimal probe geometry for near-infrared spectroscopy of biological tissue. Applied Optics 1997;36(10):2286-93.

68. Mourant JR, Bigio IJ, Jack DA, Johnson TM, Miller HD. Measuring absorption coefficients in small volumes of highly scattering media: source-detector separations for which path lengths do not depend on scattering properties. Applied Optics 1997;36(22):5655-61.

69. [Anonymous]NIRS measurement of tissue pH: optimizing small, fiber optic probe designs with the aid of Monte Carlo simulations. 2000.

70. Martens H, Naes T. Multivariate Calibration. [Anonymous]New York: John Wiley & Sons; 1989.

71. Adams MJ. Chemometrics in Analytical Spectroscopy. [Anonymous]Cambridge UK: Royal Society of Chemistry; 1995. v p.

72. Norris K, Williams P. Near-infrared technology in the agricultural and food industries. [Anonymous]St. Paul: American Association of Cereal Chemists; 1987.

73. Chance B, Liu H, Kitai T, Zhang Y. Effects of solutes on optical properties of biological materials: models, cells, and tissues. Analytical Biochemistry 1995;227:351-62.

74. Keijzer M, Richards-Kortum R, Jacques SL, Feld MS. Fluorescence spectroscopy of turbid media: autofluorescence of the human aorta. Applied Optics 1989;28:4286-92.

75. Soller BR, Micheels RH, inventors; [Anonymous] Optical measurement of tissue pH. 5,813,403. 1998 Sep 29;

76. Steinke JM, Shepard AP. Effects of temperature on optical absorbance spectra of oxy-, carboxy-, and deoxyhemoglobin. Clinical Chemistry 1992;38(7):1360-4.

77. Casscells W, Hathorn B, David M, Krabach T, Vaughn WK, McAllister HA, Bearman G, Willerson JT. Thermal detection of cellular infiltrates in living atherosclerotic plaques: possible implications for plaque rupture and thrombosis. Lancet 1996;347:1447-9.

78. Arnold MA, Burmeister JJ, Small GW. Phantom Glucose Calibration Models from Simulated Noninvasive Human Near-Infrared Spectra. Analytical Chemistry 1998;70:1773-81.

79. Haaland DM. Synthetic multivariate models to accommodate unmodeled interfering spectral components during quantitative spectral analyses. Applied Spectroscopy 999 Sep 1;54(2):246-54.

80. Stary, H. C., Chandler, A. B., Dinsmore, R. E., Fuster, V., Glagov, S., Insull, W., Rosenfeld, M., dam, Wagner, W., and Wissler, R. W. A Definition of Advanced Types of Atherosclerotic Lesions and a Histological Classification of Atherosclerosis. American Heart Association . 2000. (GENERIC) Ref Type: Electronic Citation

81. Kirk JE. Lactic Dehydrogenase. In: Kirk JE, editor. Enzymes of the Arterial Wall. New York: Academic Press; 1969. p 21-9.

82. Wang L, Jacques SL, Zheng L. CONV - Convolution for responses to a finite diameter photon beam incident on multi-layered

tissues. Computer Methods and Programs in Biomedicine 1997;54:141-50.

83. Jacques SL. [Anonymous] Tissue Optics. Oregon Medical Laser Center: SPIE. 1999 Jan 24; p.1 SC34. Short Course Notes.

84. van Staveren HJ, Moes JM, van Marle J, Prahl SA, van Gemert JC. Light scattering in intralipid-10% in the wavelength range of 400-1100 nm. Applied Optics 1991;30(31):4507-14.

85. Flock ST, Jacques SL, Wilson BC, Star WM, van Gemert JC. Optical properties of Intralipid: a phantom medium for light propagation studies. Lasers in Surgery and Medicine 1992;12:510-9.

86. van Gemert JC, Verdaasdonk R, Stassen E, Schets G. Optical properties of human blood vessel wall and plaque. Lasers in Surgery and Medicine 1985;5:235-7.

87. van Gemert JC, Welch AJ, Jacques SL, Cheong Q, Star WM. Light distribution, optical properties, and cardiovascular tissues. In: Abela G, editor. Lasers in cardiovascular medicine and surgery: fundamentals and techniques. Norwell: Kluwer Academic Publishers; 1990.

88. Prince MR, Deutsch TF, Mathews-Roth MM, Margolis R, Parrish JA, Oseroff AR. Preferential light absorption in atheromas in vitro. Implications for laser angioplasty. J Clin Invest 1986;78(1):295-302.

89. Lowry OH, Passonneau JV. Enzymatic analysis : a practical guide. [Anonymous]Totowa, NJ: Humana Press; 1993.

90. Naghavi M, Khan T, Soller B, Melling P, Asif M, Madjid M, Casscells W. pH and lactate imaging of atherosclerotic plaques: introducing a 3-french, 360-degree side-viewing, near-infrared spectroscopic catheter to monitor metabolic activity of atherosclerotic plaque. The American Journal of Cardiology 2001 Jul 19;88(1):81-.

91. Khan T, Soller B, Melling P, Madjid M, Casscells W, Naghavi M. Progress with the calibration of a 3F near infrared spectroscopy fiber optic catheter for monitoring the ph of atherosclerotic plaque: introducing a novel approach for detection of active vulnerable plaque. Journal of the American College of Cardiology 2002 Mar 6;39(1):18-.

92. Bergmeyer R. Methods of Enzymatic Analysis: Metabolites - Carbohydrates. 3rd ed. [Anonymous] 1984 Jan. 587 p.

Project I.C.4 "Nitric Oxide in Organ Failure"

Investigator: Bruce C. Kone, M.D., FACP, FCP

Body. The broad objective of this project is to explore the molecular mechanisms underlying the effects of nitric oxide (NO) and its derived reactive nitrogen intermediates to injure tissues during multiple organ failure.

Using a rat model in which gut injury and multiple organ failure are induced by 45 minutes of superior mesenteric artery occlusion followed by progressive periods of reperfusion, we examined early molecular events, including stress kinase and transcription factor activation, apoptosis, and induction of adhesion molecules and cytokines. We performed histology, analysis of pro-inflammatory genes, including inducible nitric oxide synthase (iNOS), interleukin-8, and intercellular adhesion molecule-1 in this model. We found that I/R injury promoted histological evidence of severe gut injury, impairment of intestinal transit time, evidence of activation of the pro-inflammatory genes listed above, as well as activation of the inducible transcription factor NF-kB. We further showed that a-melanocyte-stimulating hormone (a-MSH), a tridecapeptide released by the pituitary gland and immunocompetent cells, significantly limited post-ischemic injury to the rat small intestine. The data suggested the possibility that a-MSH inhibited NF-kB activation and thereby limited inflammatory injury. A paper reporting these results has been published in the *American Journal of Physiology: Gastroenterology*.

To examine the role of NF-kB in postischemic injury in the intestine, we studied the effects of an IkB inhibitor (Bay compound) that limits NF-kB activation in this model. Interestingly, the inhibitor protected against early (30 minutes of reperfusion) injury, but aggravated late (6 hours of reperfusion) injury, suggesting a role of this transcription factor not only in the acute injury process but also in the later repair process. We further showed that the late effects of NF-kB were related to activation of a novel tyrosine kinase pathway, which resulted in tyrosine phosphorylation of IkB that escaped inhibition by the Bay compound. A paper of these results has been submitted for review.

Using this same model, we examined the effects of topical hypothermia (cooling the intestine) during the I/R period. We found that this approach dramatically reduces intestinal injury and dysfunction. A paper reporting these results is in press in *Surgery*.

We also explored the role of STAT3 transcription factors in IL-1b- and LPS + IFN-g-mediated iNOS induction in murine mesangial cells. Both stimuli induced rapid phosphorylation of STAT3 and sequence-specific STAT3 DNA-binding activity. Supershift assays with a STAT3 element probe demonstrated that NF-kB p65 and p50 complexed with STAT3 in the DNA-protein complex. The direct interaction of STAT3 and NF-kB p65 was verified *in vivo* by co-immunoprecipitation and *in vitro* by pull down assays with GST-NF-kB p65 and *in vitro* translated STAT3a. Overexpression of STAT3 dramatically inhibited IL-1b- or LPS + IFN-g-mediated induction of iNOS promoter-luciferase constructs that contained the wild type iNOS promoter or ones harboring mutated STAT binding elements. In tests of indirect inhibitory effects of STAT3, overexpression of STAT3

39

dramatically inhibited the activity of an NF-kB-dependent promoter devoid of STAT binding elements without affecting NF-kB DNA binding activity. Thus STAT3, via direct interactions with NF-kB p65, serves as a dominant-negative inhibitor of NF-kB activity to suppress indirectly cytokine induction of the iNOS promoter in mesangial cells. These results provide a new model for the termination of NO production by activated iNOS following exposure to pro-inflammatory stimuli. A manuscript reporting these results has been published.

We examined the role of an E-box motif at -904/-883 of the iNOS promoter in its transcriptional induction. By using site-directed mutagenesis of the -893/-888 E-box and correlating functional assays of the mutated iNOS promoter with USF DNA-binding activities, we demonstrate the -893/-888 E-box motif is functionally required for iNOS regulation in murine mesangial cells and that upstream stimulatory factors (USFs) are *in vivo* components of the iNOS transcriptional response complex. Mutation of the E-box sequence augmented the iNOS response to IL-1b in transiently transfected mesangial cells. Gel mobility shift assays demonstrated that USFs can no longer binding to the -893/-888 E-box promoter region when the E-box is mutated. Cotransfection of USF1 and USF2 expression vectors with iNOS promoter-luciferase reporter constructs suppressed IL-1b simulated iNOS promoter activity. Cotransfection of dominant-negative USF2 mutants lacking the DNA binding domain or *cis*-element decoys containing concatamers of the -904/-883 region augmented IL-1b stimulation of iNOS promoter activity. Using gel mobility shift assays, only USF1 and USF2 supershifted the USF protein/DNA complexes. These results demonstrated that USF binding to the E-box at -893/-888 serves to *trans*-repress basal expression and IL-1b induction of the iNOS promoter. This paper was also published.

We explored the role of acetylation in cytokine-mediated iNOS induction in cultured murine mesangial cells and RAW 264.7 cells. Nitric oxide production was measured by the Griess reaction. The activity of the iNOS promoter and a NF-kB element promoter was assessed in transient transfection assays. Gel shift and supershift assays were used to identify NF-kB in nuclear extracts. Protein-protein interactions were assayed by co-immunoprecipitation and GST pull-down assays. Treatment with the HDAC inhibitor trichostatin A (TSA) and overexpression of HDAC isoforms were used to assess the impact of acetylation status on iNOS and NF-kB element promoter activity. TSA inhibited induction of endogenous NO production and iNOS as well as NF-kB element promoter activity in response to IL-1b or LPS + IFN-g in both cell types without altering NF-kB DNA binding activity. Overexpression of specific HDAC isoforms enhanced cytokine induction of both the iNOS and the NF-kB element promoter. HDAC2 and NF-kB p65 co-immunoprecipitated from mesangial cell nuclear extracts, and in vitro translated HDAC2 specifically interacted with an NF-kB p65 GST fusion protein. Hyperacetylation diminishes cytokine induction of iNOS transcription activity, at least in part, by limiting the functional efficacy of NF-kB. The specific recruitment of HDAC2 to NF-kB at target promoters and the consequent effects on acetylation status may play an important role in regulating iNOS as well as other NF-kB-dependent genes involved in inflammation.

Finally, continued our proteomic studies designed to identify novel targets for S-nitrosylation by NO. NO can S-nitrosylate cysteine residues in target proteins, potentially altering their functional

activity. Mesangial cell lysates were treated with vehicle or the NO donors SNAP or S-nitrosoglutathione. Treatment with reduced glutathione served as a negative control. The lysates were then subjected to the "biotin switch" method and the resulting isolated population of S-nitrosylated proteins was analyzed by MALDI-TOF mass spectrometry. Using this technique we have identified 37 proteins not previously known to be modified by S-nitrosylation. A manuscript reporting these results is in preparation, and an abstract has been selected for presentation at the November 2002 Annual Meeting of the American Society of Nephrology.

Key Research Accomplishments

- Characterization of the beneficial and deleterious effects of selective NF-kB inhibition in the post-ischemic intestine

- Demonstration of a therapeutic effect of intraoperative topical hypothermia to abrogate intestinal injury following ischemia-reperfusion

- Demonstration that STAT3 interacts with NF-kB and thereby inhibits iNOS transcriptional activation

- Demonstration that that USF1 and USF2 are novel transcriptional inhibitors of iNOS

- Demonstration that NF-kB p65 interacts with histone deacetylases and thereby participates in the control of iNOS transcriptional induction.

- Demonstration of 37 novel proteins S-nitrosylated by NO

Reportable Outcomes

Articles:

Hassoun, H.T., Zou, L, Moore, F.A. Kozar, R., Weisbrodt, N.W., and Kone. B.C.: a-Melanocyte stimulating hormone protects against mesenteric ischemia/reperfusion injury. Am. J. Physiol. 282: G1059-G1068, 2002.

Yu, Z., Zhang, W., and Kone, B.C Histone deacetylases augment cytokine induction of the iNOS gene. J. Am. Soc. Nephrol 13:2009-2017, 2002.

Yu, Z., Zhang, W., and Kone, B.C Signal transducers and activators of transcription 3 (STAT3) inhibits transcription of the inducible nitric oxide synthase gene by interacting with nuclear factor kB. Biochem J. 367:97-105.

Gupta, A.K., and Kone, B.C.: USF-1 and -2 *trans*-repress IL-1b-induced iNOS transcription in mesangial cells. Am. J. Physiol: Cell, in press.

Hassoun, H.T., Kozar, R.A., Kone, B.C., Safi, H.J., and Moore, F.A.: Intraischemic hypothermia differentially modulates oxidative stress proteins during mesenteric ischemia/reperfusion. Surgery, in press.

Abstracts:

Kuncewicz, T., Sheta, E., Goldknopf, I, and Kone, B.C. Proteomic

analysis reveals novel protein targets of S-nitrosylated in mesangial cells. 35th Annual Meeting of the American Society of Nephrology, Chicago, IL 2002.

Yu, Z-Y., Zhang, W., and Kone, B.C. Stat3 inhibits transcription of the inducible nitric oxide synthase gene by interacting with NF-kB. 35th Annual Meeting of the American Society of Nephrology, Chicago, IL 2002.

Yu, Z-Y., Zhang, W., and Kone, B.C. Hstone deacetylases augment cytokine induction of the inducible nitric oxide synthase gene. 35th Annual Meeting of the American Society of Nephrology, Chicago, IL 2002.

Kone, B.C., and Gupta, A.K.: USF-1 and -2 trans-repress IL-1b-induced iNOS transcription in mesangial cells. 35th Annual Meeting of the American Society of Nephrology, Chicago, IL 2002.

Conclusions

Multiple organ failure is a common, often catastrophic outcome of combat-induced trauma. An improved understanding of the molecular basis for the initiation and amplification of cell and organ injury will ultimately inform the rational design of therapeutic agents to prevent, delay, or reverse post-resuscitation multiple organ failure. Collectively, our studies provide new insights into the early molecular mechanisms underlying both intestinal ischemia-reperfusion injury and multiple organ failure, new insights into the transcriptional regulation of iNOS, and novel insights into the protein targets of NO that may function in nitrosylation-sensitive signal transduction and transcription pathways. Since many organ systems are susceptible to ischemia-reperfusion injury and nitrosative stress, these results should provide insights into pathophysiologic mechanisms in the heart, kidney, lung, and liver.

Project I.C.6. "Is Hypothermia an Indicator of Imminent Death in Congestive Heart Failure, Helpful in Triage"

Investigator: S. Ward Casscells, M.D.

As presented earlier in project proposals to the U.S army, we had found that *Hypothermia* was a predictor of imminent death in patients with congestive heart failure. This report summarizes the developments in this field and plans for future research.

Clinical study: As outlined in the proposal, a cohort study involving 326 subjects was undertaken by the group. Hospital charts of 291 CHF patients belonging to the Memorial Hermann Hospital in Houston were reviewed for common clinical predictors of CHF mortality and core body temperature. Univariate and multivariate analyses were done to investigate predictors of in-hospital mortality. On multiple regression analysis, hypothermia was the strongest predictor of death, followed by ventricular tachycardia. Also, hypothermia appears to be a novel predictor of imminent death in these patients, in both univariate and multivariate models.

The manuscript of this study has been submitted to the Journal of The American College of Cardiology for publication.

This study concluded that hypothermia predicted in-hospital death in these CHF patients and once confirmed by further studies, this finding should prove useful, because temperature can be measured continuously, rapidly and inexpensively in or out of the hospital, in disaster relief medical care units and in battle field triage units.

New inventions based on the study: The data from the above mentioned study was further analyzed in an exploratory manner, which further concluded that steep changes in core body temperature predicted and well preceded in-hospital death in CHF patients. From this we hypothesized that the sensitivity and specificity of this previous hypothermia predictive tool might be improved by more frequent and uniform measurement, by combining temperature with other variables. We conclude that ambulatory temperature monitoring in CHF patients merits further investigations. Based on this new discovery, we, on September of 2002, filed a continuation in part (CIP) to the original patent that was filed before the funding of this project.

The filed CIP generally relates to apparatus and methods for continuous monitoring of health condition of patients with congestive heart failure. It involves detecting a significant worsening of condition of a CHF patient and issuing an alert so that life saving therapies and interventions can be summoned to save the patient's life and/or intervention devices can be activated or adjusted. In an aspect of the invention, the output of an alert is to a medical device that applies a therapeutic treatment to the patient to treat the patient's condition of congestive heart failure. The device suitably may be a ventricular assist device responsive to the alert to provide additional ventricular assist to the patient. The device may be a medication release device responsive to the alert to adjust the amount of medication the patient is receiving. Or the device may be a cardiac rhythmic regulator, such as a pacemaker or defibrillator, responsive to the alert to optimize the patient's regulator parameters to reverse hypothermia, or a device responsive to the alert to warm the patient. In a significant departure from use of other prognostic factors, these new methods and apparatus not only are dynamically predictive but also are applicable for

watching the individual patient on an ambulatory and continuous basis, allowing the patient to be monitored at home as well as in-hospital or elsewhere in the emergency care units. This allows protects the patient by enabling immediate availability of professional care appropriate to his or her condition for timely initiated therapy or intervention the patient, as well providing the patient with an improved quality of life.

The main goals of our invention are:
- To accurately predict, in a CHF patient, when a significantly worsening condition signifying death draws near.
- Give sufficient warning so that steps can be taken to save them.
- To set criteria for selection of CHF patients in the very poorest condition for heart transplantation or left ventricular assist device (LVAD) implantation by knowing which patients are likely to have the shortest lives.

Our invention involves detecting a significant worsening of condition of a CHF patient and issuing an alert so that life saving therapies and interventions can be summoned to save the patient's life and/or intervention devices can be activated or adjusted. In an aspect of the invention, the output from the alert is to a medical device that the method means, apparatus and systems alert a worsening of condition in a patient with congestive heart failure. The operations of such a system include:
- Pre-setting a cut-off point of at least one temperature attribute of hypothermia comprising of a rate of fall of body temperature relative to optimum sensitivity and specificity, for such attribute as congestive heart failure, as a predictor of death in a patient.
- Routinely determining that attribute in the patient.
- Analyzing from the routine determinations of the attribute whether a condition of congestive heart failure hypothermia has occurred.

Independent confirmation: the team is trying to collaborate with other investigators around the United States and elsewhere who are involved in ongoing CHF clinical trials to test the hypothesis on their databases. We are negotiating with SCIOS Inc. to analyze their database and with Memorial Hermann Home Health to further study the concept in a prospective and also retrospective manner.

Previously, a pilot study on all patients who got LVAD implant as a bridge to transplant in SLEH and THI was launched based on the hypothesis that falling temperatures before the implantation of LVAD predicts poor outcomes of LVAD implantation in CHF patients. After doing a pilot analysis, this study was placed on hold based on the observations that the effect of in-house rise in temperature of the patients confounded the variables and that the criteria used by the surgeon in the implantation of the devices did not match our study.

Prototype development: we are seeking assistance from TenX and Fairway Medical in developing a prototype to aid in the proof of concept. We are also actively recruiting engineers to assist us with our projects and in-house consultation.

Commercialization of the concept: Based on the above mentioned research, a company by the name of LifeSentry has been incorporated. LifeSentry's technology is targeted to be used on the continuous serial measurements of temperature from one or several places in (or on) the

patient's body. Measurements are compared, averaged, digitally filtered, and otherwise processed; and if the patient is deemed at risk, an "alert" is activated; such alerts being patient alerts, monitored alerts, or both. LifeSentry's "alerts" also will be electronically linked to medical care professionals, via telemedicine technology, providing enhanced opportunities for early interventions. This technology if successful might be used at home, in hospitals, emergency rooms, intensive care units, disaster relief medical care units or triage in the battle fields.

References
1. Casscells W, **Payvar S**, Vaseghi MF, Siadaty MS, Madjid M, Siddiqui H, Lal B, Naghavi M. Hypothermia Is a Bedside Predictor of Imminent Death in Patients with Congestive Heart Failure. Under review for publication in *Journal of the American College of Cardiology*.

2. Casscells S. W., **Payvar S**. Method and Apparatus for Continuous Temperature Monitoring to Indicate Worsening of Health of Congestive Heart Failure Patients. USPTO patent pending.

3. Nohria A, Lewis E, Stevenson LW. Medical management of advanced heart failure. JAMA. 2002 Feb 6; 287(5):628-40.

Project I.D. "Up-regulation of P450 – A Natural Broad Based Defense Against Chemical and Biological Threats"

Investigator: Henry W. Strobel, Ph.D.

During the past year we have continued our focus on the response of lung to injury - chemical, biological and traumatic. Our primary focus has been on the role played by the cytochromes P450 4F in response to injury. Our work has necessitated the expression and characterization of the cytochromes P450 4F present in animal models (rats and mice) as well as in humans. Our work supported by this award, characterizing the CYP 4F5 gene has just been published in Gene and a copy of that publication is included with this report. The preparation of the genomic clone, the characterization of the intron exon boundaries and an evaluation of the promoter region in the 5_ flanking segment are presented in this manuscript.

In addition to the publication of the CYP 4F5 gene structure, we have focused on further characterization of the regulation of CYP 4Fs following chemical, biological or physical challenge. In a paper accepted for publication in BBA (Expression of Cytochromes P450 4F4 and 4F5 in Infection and Injury Models of Inflammation, Cui, et al, 2002), we report a two-phase response to injury. In the first 24 hours after insult cytochromes P450 4F4 and 4F5 decline to reach a low point of expression at 24 hours post injury. The second or recovery phase extends from 24 hours to 2 weeks post insult and is marked by a rise in 4F4 and 4F5 to pre-injury levels and above. This rise is definable by 4F mRNA expression as well as by changes in 4F protein levels. The response pattern is similar whether the insult is biological, chemical or physical. When lipopolysacihande is used as the injury agent, the suppression of CYP 4Fs in 24 hours is dose-dependent. When blunt trauma is the injury the same pattern is observed.

Most remarkable are the effects of specific local injury on the whole body. One might expect a widespread response following systemic injection of a chemical or biological injury agent. We have observed, however, that the injury and recovery periods follow the same time frame in **lung** tissue and liver tissue as they do in brain when the injury stimulus is a controlled blow to the temporal cortex of a sedated rat. In other words, with no observable delay, the response to injury occurs at the site of injury as well as at sites quite distant and effectively separate (in terms of general function, innervation, blood supply and hormonal regulation) from the site of injury.

While we have observed this in terms of effects on CYPs 4F and cyclooxygenase II we are now defining these changes at the level of leukotriene B_4 and prostaglandin A_1 and E_1 (products of lipopolysacihande 5 and cyclooxygenase II) and at the level of lipoxygenase 5 expression as well as IL1, IL6 TNF_α results will contribute to defining both the widespread changes in inflammatory signals across the tissues as well as in the signals for these changes. We feel this picture will help define post injury traumatic changes in organ system function and indicate modes for improved treatment of battlefield and disaster injuries.

During this Dr. Yasushi Kikuta has succeeded in developing a CYP 4F14 knockout mouse. At this stage we have chimeric mice that will be bred to produce the F1 generation of heterozygous (CYP 4F14 $^+/-$) mice.

We will then analyze these mice phenotypically and challenge the homozygous and heterozygous mice with chemical, biological and physical insults.

Cui, Xiaoming, Strobel, Henry W.: "Cloning and characterization of the rat cytochrome P450 4F5 (CYP4F5) gene" *GENE*, in press, 2002.
Cui, X, Kalsotra, A., Robida, A.M., Matzilevich, D., Moore, A.N., Boehme, C.L., Morgan, E.T., Dash, P.K., and Strobel, H.W.: "Expression of Cytochromes P450 4F4 and 4F5 in Infection and Injury Models of Inflammation," *BIOCHEMICA ET BIOPHYSICA ACTA,* in press 2002.

Project I.E. "Detection and Quantitation of *Bacillus anthracis* in Macrophages"

Investigator: Theresa M. Koehler

Introduction

Anthrax disease results from a complex series of interactions between the invading bacterium, *Bacillus anthracis*, and the mammalian host. For inhalation anthrax, infection begins with entry of spores into the lung. The spores are phagocytosed by alveolar macrophages and transported to the lymph nodes of the mediastinum. Ultimately the metabolically active form of the bacterium disseminates to the blood and other body tissues, reaching concentrations of approximately 10^8 CFU per ml and secreting the anthrax toxin proteins. Synthesis of the anthrax toxins by *B. anthracis* is essential for pathogenesis resulting in anthrax disease and in recent years, much information has been gained from studies of toxin protein structure and function. However, anthrax disease, whether acquired naturally or as the result of intentional dissemination of spores, results from infection with *B. anthracis*, not simply acquisition of toxin. Despite the importance of human infection with *B. anthracis*, little is known about the fundamental cellular and molecular mechanisms by which the bacterium interacts with its host. For example, the mechanisms for spore germination, survival in the hostile intracellular environment of the macrophages, and dissemination to other body tissues are virtually unexplored. Understanding these early steps in *B. anthracis* infection is crucial for developing strategies for attenuating or blocking the course of *B. anthracis*-mediated disease in the host. We are primarily interested in the critical early step of pathogenesis in which *B. anthracis* spores interact with macrophages.

Results

1. Development of a DNA-based method to measure growth of *B. anthracis* in macrophages.

In our last report, we described the development of real-time fluorescent quantitative PCR as a rapid and quantitative method to measure changes in the number of *B. anthracis* cells in a given sample. Using our assay, we demonstrated that the relative amounts of PCR product detected in a pure bacterial culture correlate with bacterial cell mass.

During the most recent report period, we attempted to use this assay to quantity the number of copies of a specific *B. anthracis* DNA sequence in infected macrophages, thus allowing us to assess bacterial growth in macrophages. In our experiments, we infected macrophages with *B. anthracis* spores at a multiplicity of infection of 10:1. After allowing time for adherence and phagocytosis, gentamycin was added to kill non-phagocytosed germinating spores and extracellular bacteria. At hourly time points up to 7 hours post gentamycin treatment, the culture medium was removed, cells were treated with the detergent Triton X, and samples were tested for relative amounts of the specific DNA target using our quantitative PCR method. Our experiments did not result in significantly significant data.

The major technical difficulty is the adherence of numerous *B. anthracis* spores to the surface of cultured macrophages. We are unable to remove these spores by washing. Moreover, the gentamycin treatment does not result in loss of spore viability. The numerous spores that

remain at the cell surface following infection result in a very high background, invalidating our results for intracellular bacterial DNA content.

2. Microscopic assessment of bacteria-macrophage interactions.

An alternative means of quantifying *B. anthracis* cells associated with a population of macrophages would be to generate fluorescent bacteria and measure growth as an increase in fluorescence. In addition, growth of *B. anthracis* inside macrophages could be assessed using confocal microscopy. In the previous reporting period, we determined that *B. anthracis* can express *gfp*, the green fluorescent protein (GFP) gene, and that constitutive synthesis of GFP does not affect growth rate in batch culture. During the most recent reporting period, we created a *B. anthracis* mutant harboring *gfp* under the control of a *B. anthracis* promoter, P*inhA*, on a multicopy plasmid. The mutant produces GFP throughout growth in liquid culture. Vegetative cells of this mutant, which is highly fluorescent are shown in figure 1.
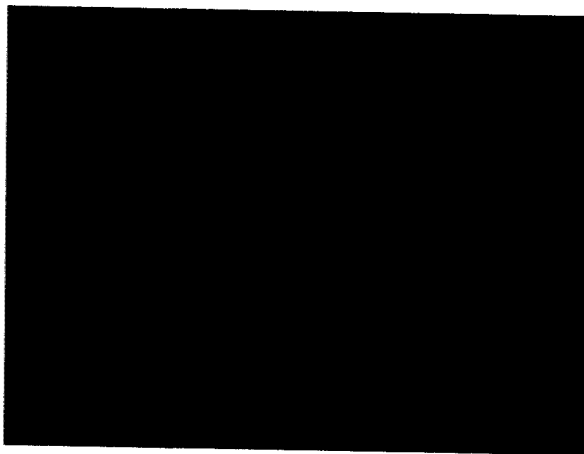

Figure 1.
B. anthracis vegetative cells producing GFP

Surprisingly, spores of the mutant are also highly fluorescent, indicating that the GFP is very stable and remains associated with spores during development. Fluorescent spores are shown in figure 2. The fluorescent spores will facilitate visualization of phagocytosis of spores by cultured macrophages.
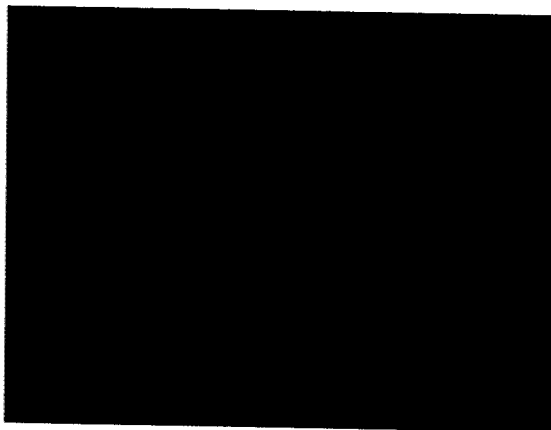

Figure 2.
B. anthracis spores containing GFP

3. Studies of a cholesterol-dependent cytolysin produced by *B. anthracis*.

In order for the pathogenesis of anthrax disease to progress beyond infection of alveolar macrophages, vegetative cells of *B. anthracis* must escape the confines of the macrophage and be released into the extracellular milieu. The mechanisms by which this occurs remain unknown. In collaboration with Richard Rest of Drexel University College of Medicine, we have identified a gene of *B. anthracis* that is associated with synthesis of a cholesterol-dependent cytolysin (CDC). CDC's represent a large family of highly conserved, pore-forming proteins that are produced by many Gram-positive pathogens, including *Listeria monocytogenes*, *Streptococcus pyogenes*, and *Streptococcus pneumoniae*. CDCs are secreted by bacteria, bind to cholesterol in host cell plasma membranes, insert into the membranes and oligomerize to form large pores. Formation of this pore is responsible for the hemolytic and cytolytic properties of CDCs. Some CDC's have been shown to play important roles in pathogenesis. The CDC of *Listeria monocytogenes*, termed listeria lysin O (LLO) contributes to the virulence of *L. monocytogenes* by allowing this organism to escape from the phagolysosome of a host macrophage. Thus, we hypothesize that the *B. anthracis* CDC, which we are calling anthrolysin O (ALO), may be playing a similar role in the pathogenesis of anthrax.

Studies in Dr. Rest's laboratory revealed that a hemolysin secreted by *B. anthracis* possesses characteristics of a CDC. An *alo*-null mutant constructed in our laboratory does not produce the hemolysin. The amount of hemolysin produced is highly dependent on the type of growth medium used. The data suggest that expression of ALO is under strict and tight environmental control. We are currently carrying out experiments to investigate the regulation of the alo gene. In future studies, we will deterine whether the *alo* gene is required for escape of *B. anthracis* from the macrophage

Key Research Accomplishments:

* Construction of a highly fluorescent *Bacillus anthracis* strain suitable for assessment of bacterial cell growth in the macrophage environment.
* Construction of a mutant B. *anthracis* strain deleted for the *alo* gene that encodes a cholesterol-dependent cytolysin. The strain will facilitate testing of the hypothesis that the cytolysin plays a role in escape of *B. anthracis* cells from macrophages.

Reportable Outcomes:

* A manuscript describing the cholesterol-dependent cytolysin of *Bacillus anthracis* is in preparation. A draft of the abstract follows.

Jeffrey G. Shannon[1], Cana Ross[2], Theresa M. Koehler[2] and Richard F. Rest[1]

[1]Department of Microbiology and Immunology,
Drexel University College of Medicine, Philadelphia, PA 19129
[2]Department of Microbiology and Molecular Genetics
University of Texas Medical School, Houston, TX   77030

Among its arsenal of virulence factors, *Bacillus anthracis* expresses two toxins intimately involved in its pathogenesis. We have investigated an additional putative toxin of *B. anthracis*, a member of

the cholesterol-dependent cytolysin (CDC) family, which includes cereolysin O, listeriolysin O (LLO) and streptolysin O (SLO). We have named the *B. anthracis* CDC anthrolysin O, or ALO. Although *B. anthracis* is generally described as expressing little or no hemolytic activity on sheep blood agar, we have shown that Sterne strain 7702 expresses significant amounts of hemolysin, i.e. ALO when grown in BHI broth, or other rich bacteriologic media, but secretes barely detectable amounts of ALO grown in Luria-Bertani Broth (LB). Growth in LB with increasing concentrations of glucose increased the amounts of hemolysin secreted into the growth medium. Expression of ALO appears to be maximal during mid- to late log phase growth, and decreases late in stationary phase. These observations are supported by real time reverse transcriptase PCR of *alo* mRNA. Hemolytic activity of ALO was increased in the presence of reducing agent, and inhibited in a dose dependent manner by cholesterol, both activities characteristic of members of the CDC family of toxins. Lytic activity of ALO against human erythrocytes was greater than against sheep erythrocytes. A mutant of Sterne strain 7702, in which the *alo* gene was deleted and interrupted by an antibiotic resistance gene, secreted barely detectable hemolytic activity. This suggests that ALO is the major active hemolysin expressed and secreted by *B. anthracis* under the conditions investigated in these studies.

Project II.A. "Pathology Core"

Investigator: James T. Willerson, M.D., L. Maximilian Buja, M.D.,
                 Silvio H. Litovsky, M.D.

   2.   A.   Pathology Core

In the DREAMS program, we have provided expert pathology assessment of
various human and animal tissues that are obtained as part of our
research studies.   Methods of analysis for these tissues include
routine   gross   morphology,   histology,   lipid   analysis,
immunohistochemistry,   electron   microscopy,   and   quantitative
morphometry.   These techniques have been extremely useful in allowing
investigators throughout the DREAMS program to evaluate tissues from
experimental animal models to make quantitative determinations that
allow them to test their hypotheses, develop their methods more exactly
and promote the development and refinement of new hypotheses.   The
pathology core interacts extensively with the DREAMS investigators to
get the maximal information from the experimental protocols and thus,
provide the best possible understanding of the pathology findings.
These analyses are available for studies of tissues, experimental
animal and human, that are obtained by investigators throughout the
DREAMS project.   In this particular part of the DREAMS program, we have
provided financial assistance for the efforts of Dr. Silvio Litovsky,
who provide most of the analyses mentioned above, as well as support
for the anatomic and laboratory pathology studies.

Project II.D. "Thermal Detection and Treatment of Inflammation and Necrosis"

Investigator: S. Ward Casscells, M.D.

Thermal Detection of Vulnerable Plaque

In 1996, we showed that inflamed atherosclerotic plaques give off more heat and that vulnerable plaques may be detected by measuring their temperature. Plaque temperature is correlated directly with inflammatory cell density and inversely with the distance of the cell clusters from the luminal surface. It is inversely related to the density of the smooth muscle cells. We found no significant association between temperature heterogeneity and presence of Chlamydia *pneumoniae* in plaque or the gross color of human atherosclerotic carotid plaques. We also found pH heterogeneity in plaques from human carotid artery and aortas of Watanabe atherosclerotic rabbits and Apo E deficient mice. Areas with lower pH had higher temperature and areas with a large lipid core showed lower pH with higher temperature, whereas calcified regions had lower temperature and higher pH. We also developed a thermography basket catheter and showed *in vivo* temperature heterogeneity in atherosclerotic lesions of atherosclerotic dogs and Watanabe rabbits. Thermal heterogeneity was later documented in human atherosclerotic coronary arteries. Temperature difference between atherosclerotic plaque and healthy vessel wall is related with clinical instability. It is correlated with systemic markers of inflammation and is a strong predictor of adverse cardiac events after percutaneous interventions. Thermography is the first in a series of novel "functional" imaging methods and is moving to clinical trials. It may be useful for a variety of clinical and research purposes such as detection of vulnerable plaques and risk stratification of vulnerable patients.
From ancient times, heat has been recognized as one of the four cardinal signs of inflammation (along with pain, swelling, and redness). We hypothesized that foci of inflammation in atherosclerotic plaques give off more heat and may be detected by measuring their temperature. We tested our hypothesis in *ex vivo* and *in vivo* settings.

Mechanism of Heat Production in Atherosclerotic Plaques

Macrophages are metabolically active cells with a very high turn-over rate of ATP. [3] In addition to oxidative reactions in the cytosol, they strongly express mitochondrial uncoupling proteins (UCP) -2 and UCP-3. UCPs are homologues of thermogenin (UCP-1), which is responsible for thermogenesis in brown fat tissue. [4] High metabolic rate and consumption of glucose and oxygen, may lead not only to increase in plaque temperature, but also, accumulation of lactate, due to anaerobic metabolism. Also, hypoxemia in plaque could contribute to the decrease in plaque pH.

Ex Vivo Thermal Detection Studies

In 1996, for the first time, we showed that there is marked temperature heterogeneity over plaque surface and that "hot plaques" are inflamed. We measured the intimal surface temperatures at 20 sites of 50 samples of carotid artery taken at endarterectomy from 48 patients. [5] Surface temperature of plaques at different points showed marked and reproducible heterogeneity (with temperature differences of 0.2-2.2 °C). Temperature correlated positively with cell density and inversely

with the distance of the cell clusters from the luminal surface. Most cells were macrophages.[5] Later, in another series of experiments, we found a close correlation between heat and the density of macrophages ($r = 0.66$; $p = 0.0001$). In contrast, the temperature was inversely related to the density of the smooth muscle cells ($r = -0.41$; $p = 0.0001$). To assess the possible contribution of infections to generation of hot plaques, we used the genus-specific monoclonal antibody CF-2 against Chlamydia *pneumoniae*. We found no significant association between temperature heterogeneity and *Chlamydia pneumoniae*. Also, gross color of the lumen surface of human atherosclerotic carotid plaques could not predict the underlying temperature. Next, we incubated the plaques with indomethacin (1 mg/mL). Indomethacin caused a gradual decrease in plaque heat production over 5 hours suggesting inflammatory origin of heat production in atherosclerotic plaques.

Our detection of thermal heterogeneity with a thermistor led us to search for other thermal detection techniques. Therefore, we moved further to verify our results by correlating the needle thermistor measurements with the infrared thermographic camera (Santa Barbara Focalplane, Goleta, CA) measurements of temperature in human atherosclerotic plaques; the result confirmed a high correlation between the two methods ($r=0.988$; $p = 0.0001$). In those plaques, which were photographed with an infrared camera, we found that temperature was related to cell density ($r = 0.797$, $p=0.001$). There was an inverse relationship of the temperature with the depth of the cells ($r = -0.786$, $p=0.0001$).

Next, we looked for the other factors which could be used to detect inflammation in the plaques. We had hypothesized that inflamed plaques are not only "hot", but are also "acidic". In other words, vulnerable plaques would show heterogeneity both in temperature and pH. To test this hypothesis, we studied human carotid endarterectomized plaques, aortas from Watanabe atherosclerotic rabbits, and aortas from Apo E deficient mice and found that, along with temperature heterogeneity, there is marked pH heterogeneity in atherosclerotic areas (in contrast to the normal arterial wall).[6]

To confirm our findings (based on measurements by glass-type microelectrodes), we used fluorescence microscopic imaging as an adjunct method. This method, too, confirmed pH heterogeneity in both humans and Watanabe hypercholesterolemic rabbit atherosclerotic plaques (and not in human umbilical artery samples, which served as normal controls).[6] Interestingly, as hypothesized, areas with lower pH had higher temperature ($r=0.7$, $p<0.0001$), and areas with a large lipid core showed lower pH with higher temperature, whereas calcified regions had lower temperature and higher pH.[6] These studies suggested that vulnerable plaques are hot and acidic, hence opening new possibilities for their detection. To move from bench to bedside, we began our *in vivo* experiments described below.

In Vivo Thermal Detection - Animal Studies

In vivo, we used a thermistor and found a thermal heterogeneity of 1.5 to 2.0 °C inside the intact aorta of the Watanabe hypercholesterolemic rabbits. Using an infrared camera, we could also demonstrate thermal heterogeneity of the exterior of the aorta of the Watanabe rabbits (in presence of normal blood flow). We also used the infrared camera for

thermal imaging of the beating heart in a canine model of atherosclerosis and could image the blood flow and the non-uniform and heterogeneous distribution of temperature along the surface of atherosclerotic coronary arteries.[7]

These findings encouraged us to develop our "thermobasket catheter", which is a thermocouple-based catheter made of a nitinol system loaded with small and flexible thermocouples for temperature measurement of the arterial wall. We tested this system in atherosclerotic dogs and Watanabe hypercholesterolemic rabbits. Temperature heterogeneity was detected over atherosclerotic lesions found in femoral arteries of dogs and aortas of Watanabe hypercholesterolemic rabbits (while it was absent in control New Zealand rabbits and disease-free carotid arteries of the canine model).[7]

In another approach to measuring vessel wall temperature, we designed and built an infrared angio-thermography catheter (as an alternative to contact-based thermocouple catheters).[9] The current prototype consists of a 4 French (usable in coronary arteries) side-viewing catheter capable of imaging temperature of the vessel wall with a 180 degrees scope. It has 19 chalcogenide fibers (bundled hexagonally together), and a wedge-shaped mirror assembly at its tip, which is transparent to infrared radiation and capable of receiving the heat reflected from the arterial wall. The fiber optic catheter is connected to a focal plane array cooled infrared camera.[9] A real-time image reconstruction software continuously records the data and generates color-coded thermographic images of the lumen. This catheter is being tested in *ex vivo* settings.[7]

In Vivo Thermal Detection - Human Studies

In our preliminary studies, we found considerable *in vivo* thermal heterogeneity in humans by using infrared thermography during operation on atherosclerotic patients. In most cases, the indication for surgery was carotid stenosis and a transient ischemic attack or stroke. In 8 different procedures, including carotid endarterectomy, aortofemoral bypass, and femoropopliteal bypass, we demonstrated significant *in vivo* thermal heterogeneity even in the presence of blood flow.

To further investigate the role of inflammation in arterial heat production, Stefanadis and colleagues studied 60 patients with coronary heart disease (CHD) (20 with stable angina, 20 with unstable angina, and 20 with acute myocardial infarction) and 20 sex- and age-matched controls without CHD. There was a strong correlation between systemic markers of inflammation such as C-reactive protein (CRP) and serum amyloid A (SAA) with the temperature differences, suggesting that increased local heat production in coronary lesions may be due to an aggressive inflammatory response occurring in these conditions.[11]

Thermography has emerged as a useful tool in elaborating the pathophysiologic features of atherosclerosis in human. For example, Toutouzas et al. reported a good correlation between remodeling index (determined by intracoronary ultrasound) and temperature difference between the atherosclerotic plaque and the healthy vessel wall in patients with acute coronary syndromes. [12] They also showed that serum MMP-9 concentration is correlated with temperature differences in patients with acute coronary syndromes.[13] These *in vivo* studies confirm

the findings from autopsy series which showed a relation between expansive remodeling and inflammation in the plaques.[14]

Conclusion

Thermography is moving to clinical trials. It is the first in a series of novel "functional" imaging methods, which provide information about the metabolic activity of atherosclerotic plaques. If proved to be safe and reproducible, it may be used in detection of vulnerable plaques, risk stratification of vulnerable patients, and can be used by both the researchers and clinicians for variety of purposes. Simplicity of design and application of thermography, makes is a good candidate for combination with "anatomical" imaging methods for comprehensive ("*dual*") assessment of atherosclerotic lesions.[17]

Reportable Outcomes

Articles & Book Chapters:

Madjid, M., Naghavi, M., Malik, B.A., Litovsky, S., Willerson, J.T., Casscells, S.W. Thermal detection of vulnerable plaque. Am. J. of Cardiology, 2002, 90 (10, Suppl. 3): L36-L39

Madjid, M., Naghavi, M., Willerson, J.T., Casscells, S.W. Thermography: a novel approach for identification of plaques at risk of rupture and/or thrombosis. In: Fuster V (ed): Assessing and Modifying the Vulnerable Atherosclerotic Plaque. Armonk, NY: Futura Publishing Company, Inc.; 2002:107-127

Naghavi, M., Madjid, M., Gul, K., Siadaty, M.s., Willerson, J.T., Casscells, S.W. Thermography basket catheter: in vivo measurement of the temperature of atherosclerotic plaques for detection of vulnerable plaques. Submitted to Catheterization and Cardiovascular Interventions, October 2002

Acknowledgements

*Disclosure: Drs. Casscells, Willerson, Naghavi, and Madjid are shareholders in Volcano Therapeutics, Inc., a company developing diagnostic and therapeutic modalities for vulnerable plaque.

References:

1. Ross R. Atherosclerosis--an inflammatory disease. *N Engl J Med* 1999;340:115-26.
2. Shah PK. Pathophysiology of plaque rupture and the concept of plaque stabilization. *Cardiol Clin* 1996;14:17-29.
3. Newsholme P, Newsholme EA. Rates of utilization of glucose, glutamine and oleate and formation of end-products by mouse peritoneal macrophages in culture. *Biochem J* 1989;261:211-8.
4. Kockx MK, Knaapen MWM, Martinet W, De Meyer GRY, Verheye S, Herman AG. Expression of the uncoupling protein UCP-2 in macrophages of unstable human atherosclerotic plaques. *Circulation* 2000;102:II-12.

5. Casscells W, Hathorn B, David M, Krabach T, Vaughn WK, McAllister HA, Bearman G, Willerson JT. Thermal detection of cellular infiltrates in living atherosclerotic plaques: possible implications for plaque rupture and thrombosis. *Lancet* 1996;347:1447-51.

6. Naghavi N, John R, Naguib S, Siadaty SM, Grasu R, Kurian KC, van Winkle WB, Soller B, Litovsky S, Madjid M, Willerson JT, Casscells SW. pH heterogeneity of human and rabbit atherosclerotic plaques; a new insight into detection of vulnerable plaque. *Atherosclerosis* 2002;164:27-35.

7. Madjid M, Naghavi N, Willerson JT, Casscells W. Thermography: A novel approach for identification of plaques at risk of rupture and/or thrombosis. In: Fuster V, ed. Assessing and Modifying the Vulnerable Atherosclerotic Plaque. Armonk, NY: Futura Publishing Company, Inc., 2002:107-127.

8. Verheye S, De Meyer GR, Van Langenhove G, Knaapen MW, Kockx MM. In vivo temperature heterogeneity of atherosclerotic plaques is determined by plaque composition. *Circulation* 2002;105:1596-601.

9. Naghavi M, Melling M, Gul K, Madjid M, Willerson JT, Casscells W, Asif M. First prototype of a 4 French 180 degree side-viewing infrared fiber optic catheter for thermal imaging of atherosclerotic plaque. *J Am Coll Cardiol* 2001;37:3A.

10. Stefanadis C, Diamantopoulos L, Vlachopoulos C, Tsiamis E, Dernellis J, Toutouzas K, Stefanadi E, Toutouzas P. Thermal heterogeneity within human atherosclerotic coronary arteries detected in vivo: A new method of detection by application of a special thermography catheter. *Circulation* 1999;99:1965-71.

11. Stefanadis C, Diamantopoulos L, Dernellis J, Economou E, Tsiamis E, Toutouzas K, Vlachopoulos C, Toutouzas P. Heat production of atherosclerotic plaques and inflammation assessed by the acute phase proteins in acute coronary syndromes. *J Mol Cell Cardiol* 2000;32:43-52.

12. Toutouzas MK, Stefanadis CM, Vavuranakis MM, Tsiamis ME, Tsioufis MC, Pitsavos CM, P.M. T. Arterial remodeling in acute coronary syndromes: correlation of IVUS characteristics with temperature of the culprit lesion. *Circulation* 2000;102:II-707.

13. Toutouzas K, Stefanadis C, Tsiamis E, Vavuranakis M, Tsioufis C, Tsekoura D, Vaina S, P. T. The temperature of atherosclerotic plaques is correlated with matrix metalloproteinases concentration in patients with acute coronary syndromes. *J Am Coll Cardiol* 2001;37:356A.

14. Varnava AM, Mills PG, Davies MJ. Relationship between coronary artery remodeling and plaque vulnerability. *Circulation* 2002;105:939-43.

15. Stefanadis C, Toutouzas K, Tsiamis E, Vavouranakis M, Kallikazaros I, Toussoulis D, Vaina S, Voutsas A, Pitsavos C, Toutouzas P. Patients with coronary artery disease under statin treatment have decreased heat release from culprit lesions: new insights in the nonlipid effects of statins. *Eur Heart J* 2001;22:28 C.

16. Stefanadis C, Toutouzas K, Tsiamis E, Stratos C, Vavuranakis M, Kallikazaros I, Panagiotakos D, Toutouzas P. Increased local temperature in human coronary atherosclerotic plaques: an independent predictor of clinical outcome in patients undergoing a percutaneous coronary intervention. *J Am Coll Cardiol* 2001;37:1277-83.

17. Naghavi M, Madjid M, Khan MR, Mohammadi RM, Willerson JT, Casscells SW. New developments in the detection of vulnerable plaque. *Curr Atheroscler Rep.* 2001;3:125-35.

Project II.E. "Initial Evaluation of a New Axial Flow Pump, Inserted by Minimally Invasive Thoracotomy, to Maintain Cardiac Output in a Porcine Model of Cardiogenic and Hemorrhagic Shock"

Investigator: O. Howard Frazier, M.D. and Branislav Radovancevic, M.D.

Project Objectives:

The purpose of this project is to investigate a novel approach to reducing mortality and morbidity due to injuries suffered by military personnel in combat zones. Specifically, the objective of this research is to evaluate the use of an implantable mechanical cardiac assist device, in conjunction with standard volume and/or blood replacement, for treatment of hemorrhagic shock resulting from injuries sustained in the combat setting.

Progress Summary:

A total of 6 studies were performed during this reporting period. No controls were performed. Two pig studies were performed to complete the initial pig data series; the remaining 4 animals used were calves. The animals were hemorrhaged and resuscitated followed by a LVAD implant.

Control Group

No controls were performed during this reporting period.

LVAD Group

Under sterile conditions, a dual chambered polyvinylchloride catheter (Quinton) was placed in the right carotid artery. An oximetric Swan-Ganz thermodilution catheter was inserted into the external jugular and floated into the pulmonary artery for recording pressures, cardiac output, and continuous mixed venous saturation. The catheters were fixed to their respective vessels and tunneled to exit dorsally at the midline. A ventral abdominal incision was made and the spleen removed after double ligation of all vascular pedicles and the incision site closed in three suture layers. A left thoracotomy at the fifth intercostal space was performed. The Left Coronary Artery (LCA) was isolated and dissected for the placement of a 2.5 mm flow probe. The instrumentation was connected to the appropriate transducers for a 30 minutes equilibration period. Once the transducers were calibrated, the FIO2 was dropped to 30% and the animals were hemorrhaged to a mean arterial pressure (AoP) of 40 mmHg at which point it was maintained for 30 minutes to simulate a response time. After this 30-minute period, fluid administration was begun (2cc LRS/ 1cc blood loss). The animals remained under anesthesia and instrumented throughout the remainder of the study and data collected continuously.

At the end of fluid administration a double pursestring suture was placed on the descending aorta for the insertion of the outflow cannula. Another double pledgeted pursestring suture was placed in the left atria in preparation for the inflow cannula. A small incision was made, the cannula advanced into the left atria and secured with the pursestring suture. The cannulae were primed with heparinized saline and attached to fluid-primed 3/8 tubing and a centrifugal pump. The LVAD was started at a

speed of 1,000 RPM and slowly increased to provide maximum support. The animals remained under anesthesia and instrumented throughout the remainder of the study and data collected continuously.

Results

Table 1

Surgery Date	Study Type	Animal No.	Animal Wt. (kg)	Survival Time **	Amount of Hemorrhage (ml)
4/02/02	Pump	B-1362	97	26	1000
6/19/02	Pump	B-1369	122	19	1186
8/14/02	Pump	B-1378	109	38	1470
8/21/02	Pump	B-1381	110	48	775
Avg/std			104±11	33±13	932±274

Table 2
Previous Reporting period

Surgery Date	Study Type	Animal No.	Animal Wt. (kg)	Survival time**	Amount of Hemorrhage (ml)
8/9/1999	Control	B-1187	98	5.5	346
3/28/2000	Control	B-1233	102	7.5	590
8/30/2000	Control	B-1261	91	2	650
9/20/2000	Control	B-1264	109	25	992
Avg/std			100±8	10±10	645±266

**Begins at end of Hemorrhage (Hrs.)

The data from the LVAD studies were compared to previous control calf studies (Table 2) performed in previous reporting periods. The results from the calves studies performed during this reporting period are shown in Table 1. The average weight for the LVAD group was 104±11 kg and 100±8 kg for the control group. The amount hemorrhaged for the LVAD group was 932±274 ml compared to 645±266 ml for the control group. The survival time for the LVAD group was 33±13 hrs and 10±10 for the control group.

Summary

All calves survived the surgical procedure and subsequent hemorrhage. In order to achieve a mean blood pressure of 40 mmHg in the LVAD group a greater, though not significant, blood volume was bled from the animals than the control. After 30 minutes of simulated response time, fluid resuscitation was performed for the control. In addition to the fluid resuscitation, the experimental group was implanted with a LVAD.

60

Mean survival rate of the control group was only 10 ± 10 hours and significantly shorter than in the LVAD group 33± 13 (p<0.05). Three of the LVAD studies survived until or beyond the protocol endpoint (24 hours). We have developed a pressure-fixed hemorrhagic shock model in calves, which is prolonged, reproducible, and leads to certain death despite the use of drugs and fluid resuscitation. It appears that combining the use of a LVAD with standard fluid resuscitation may improve the chances of survival.

Project II.F. "Physiological Magnetic Resonance Imaging"

Investigator: James T. Willerson, M.D., Morteza Naghavi, M.D., Silvio H. Litovsky, M.D.

Noninvasive Magnetic Resonance Imaging of Macrophage Infiltration in Atherosclerotic Plaques Using Superparamagnetic Iron Oxide Nano-Particles

INTRODUCTION

In the past decade, enormous progress has been made in using MRI to visualize atherosclerotic plaques. Clinically, MRI may be used to identify atherosclerotic plaques not only in major arteries (aorta and carotid)[7], but also in small arteries (coronaries).[8] However, the resolution at which coronary plaques can be studied is limited and largely affected by the anatomical and physiological variables influencing the coronary arteries.[9] Although MRI is a powerful tool for detailing plaque morphology and structure (i.e., fibrous cap, lipid core, intraplaque hemorrhage, and calcified areas), focusing only on the morphological and structural features of atherosclerotic plaques may not be enough. The frequency of benign atherosclerotic plaques is well known from autopsy [10,11] and from intravenous ultrasound (IVUS) studies,[12,13] and this has raised an important question: Is every plaque with a lipid core and a thin cap at risk of complication? A reliable clinical test for vulnerable plaques will ideally provide information related to plaque morphology and plaque physiological and metabolic activity[14,15] because (1) abnormal activity precedes abnormal morphology, and (2) plaques with similar morphologies may not be similarly active and therefore may lead to different outcomes (i.e., more active plaques are more likely to cause complications).

The following MRI techniques may provide information beyond morphological definitions: (1) MRI using traditional, function-specific, or antibody-labeled plaque-targeted contrast media; (2) MR spectroscopy; (3) functional (blood oxygen level-dependent, or BOLD) MRI; (4) MR thermometry; (5) MR elastography; and (6) shear-stress MRI (phase-contrast MRI).[16] Another possible contributor is conventional MRI that uses the specific blood pool contrast agent superparamagnetic iron oxide (SPIO). SPIO particles, which are 50-to-100-nm in size, can be coated with a variety of biocompatible materials. They have a strong T2-shortening effect and are currently used in clinical diagnosis of hepatic tumors and metastases in lymphatic vessels. A smaller, longer-circulating type called ultra-small SPIO has been used in experimental animal models to detect inflammation associated with graft rejection[17,18] and encephalitis.[19] It has also been shown that SPIO is more avidly taken up by monocytes and macrophages than by other cells.[20] In the present study, we tested the hypothesis that SPIO particles accumulate in atherosclerotic plaques inside macrophages and that SPIO-enhanced MRI can noninvasively identify inflamed atherosclerotic plaques.

MATERIALS AND METHODS

Experimental Animals

For the experiments described below, ApoE-deficient and C57BL/6 mice (10-14 months old), Watanabe hereditary hypercholesterolemic (WHHL) rabbits (2-3 years old), and New Zealand White (NZW) rabbits (1-2 years old) were used. All experimental procedures in these animals

were performed in accordance with protocols approved by the Institutional Animal Care and Research Advisory Committee at each participating center.

SPIOs

Four types of SPIO (50-100 nm) were used in our experiments. Three of them were developed in our laboratories: uncoated SPIO (SPIO-1), lipid-coated SPIO (SPIO-2), and dextran-coated SPIO (SPIO-4). The fourth was a commercially available dextran-coated SPIO (Feridex, Berlex Laboratory, New Jersey), designated SPIO-3 for our purposes.

Studies of SPIO Uptake by Macrophages

In Vitro

Peritoneal macrophages were obtained from Balb/C mice by intraperitoneal injection of 0.1 mg of pristine (mineral oil). After 2 days, the mice were sacrificed, the peritoneum opened, and macrophages extracted by peritoneal lavage and plated at a density of 10^4 macrophages/well in triplicate on a 96-well plate. Doubly diluted fluorescein isothiocyanate (FITC)-labeled SPIO was added such that the concentration of SPIO was lowered from 10 to 0.6 _g/ml. Cells were incubated for 24 hours, washed 3 times with sterile warm PBS, lysed with 0.1% saponin, and analyzed under a Fluoroskan Ascent reader (Labsystems, Helsinki, Finland) for fluorescence at wavelengths of 485 nm and 530 nm. Fluorescence was expressed in average fluorescence units (AFU) $\pm$ SD per dose (each 100 ng of FITC-labeled SPIO = 1 AFU). Three independent experiments were performed.

In Vivo

Peritoneal macrophages

Mouse peritoneal macrophages were elicited as described above. After 2 days, FITC-labeled SPIOs, including SPIO-1, SPIO-2, and SPIO-3 were injected intraperitoneally in mice. Twenty-four hours later, peritoneal macrophages were harvested by washing and then plated in slide chambers or tissue flasks. Twenty-four to 48 hours after culture, the cells were washed and fixed with 3% paraformaldehyde. Fixed cells were then examined under a Fluoroskan Ascent reader (Labsystems) for fluorescence detection at wavelengths of 485 nm and 530 nm.

Circulating blood

Three ApoE-deficient mice were injected with SPIO-3 (0.5 mmol/kg) via the tail vein. Blood samples were taken at several points during the 6-12 hours after SPIO-3 injection and stained with Perls' staining to identify iron-positive leukocytes.

Studies of Intracellular Induction of Oxidative Stress

In order to evaluate the uptake of different SPIOs (see below) and their induction of oxidative stress, 2 series of experiments were done. In one series, mouse peritoneal macrophages were isolated in culture medium, incubated with different SPIOs for 4 hours, and then

washed. After 24 hours, the nitric oxide (NO) content of the supernatant was measured in supernatant using the Greiss reagent. In the second series of experiments, SPIOs fluorescently labeled with FITC were added to macrophages in the presence of 2 inhibitors of the mannose receptor, mannan and dextran. Intracellular retention of fluorescently labeled SPIO was measured after 2 hours.

Studies of Intracellular SPIO Relaxivity

The T2-shortening effect of intracellular SPIO was evaluated at 4 different time points using 4 different concentrations of SPIO-3. In brief, 10×10^5 macrophages were added to each of 4 tubes containing 50, 100, 250, and 500 nmol Fe/ml diluted, respectively, and 2 control tubes containing macrophages but no SPIO and then incubated for varying periods. At several time points (20 min, 1 hour, 6 hours, and 24 hours), 6 tubes (4 containing SPIO at different concentrations and 2 containing controls) were centrifuged at 1000 rpm for 5 minutes, washed with PBS for 5 minutes, and then fixed in paraformaldehyde. This resulted in 24 tubes of macrophage for analysis. Finally, the tubes were stacked and scanned in a 7.1T MRI scanner (Bruker).

Pathologic Examination of In Vivo Distribution of SPIO in ApoE-Deficient (Atherosclerotic) vs. Wild-type (Control) Mice

In order to study the distribution of SPIO in atherosclerotic versus normal mice, 7 ApoE-deficient (atherosclerotic) mice and five C57BL/6 (control) mice were injected with SPIO-3 (1 mmol Fe/kg) via the tail vein. The mice were sacrificed on postinjection days 3 and 5. Tissues from different organs (including the liver, spleen, kidneys, lung, heart, and bone marrow) and from aortas (including the valvular, ascending, descending, and abdominal regions) were fixed and sent for staining and pathological examination. Stains used were hematoxylin and eosin (H&E), Perls' (iron), and CD68 and MAC-2 (macrophage). After iron staining, the atherosclerotic aortic walls of the ApoE-deficient mice were compared with the normal aortic walls of the C57BL mice in terms of the number of iron particles per high power field.

Histopathological Examination of In Vivo Distribution of SPIO in Rabbits

In order to study the distribution of iron in different tissues, 4 WHHL rabbits and 2 NZW rabbits (controls) were injected with SPIO-3 (2 mmol Fe/kg) IV through an ear vein. One WHHL and one NZW rabbit served as untreated controls (i.e., they received no SPIO). Animals were sacrificed on postinjection day 5. Tissues from the aorta as well as liver, spleen, kidneys, and heart were fixed and stained for H&E, iron, and RAM 11 (rabbit anti-macrophage antibody).

Comparison of Pre and Post-Contrast MRI Scans

ApoE-deficient vs. Normal Mice

4.7T MRI scanning

Using a 4.7T MRI scanner (Bruker) with respiratory gating, baseline MRI was performed on 6 ApoE-deficient and 2 wild-type mice (TR = 2500 msec, TE = 12 msec, FOV = 6.6 cm, slice thickness = 2.0 mm, flip

angle (orient) = trans, and matrices = 256 x 256 pixels). The mice were then injected with SPIO-3 (1 mmol Fe/kg) IV via the tail vein. Post-contrast MRI was performed on day 5 using the same MRI parameters. Pre-contrast (baseline) and post-contrast images of the aorta at the renal level were compared.

7T MRI scanning

Using a 7 T MRI scanner (Bruker) with respiratory and ECG gating, baseline MRI was performed on 5 ApoE-deficient and 2 normal mice (TR = 2500 msec, TE = 32 msec, FOV = 2.5 cm, slice thickness = 1.0 mm, and matrix = 512 x 512 pixels). The mice were injected with SPIO-3 (1 mmol Fe/kg). Post-contrast MRI was performed on day 5 using the same MRI sequences. Pre-contrast (baseline) and post-contrast images of the aorta at the root and renal artery ostia were compared.

WHHL vs. NZW Rabbits

In Vivo

Using a 1.5T MRI system (Signa, General Electric) equipped with a conventional extremity coil, baseline MRI of the aorta was done in 4 WHHL and 2 NZW rabbits (T2 gradient echo: TR = 1200 msec, TE = 6 msec, FOV = 16 x 12 cm, matrix size = 256 x 192 pixels; 3-dimensional magnetic resonance [3D MR] angiography with gadolinium-DTPA: TE = 1.3 msec, TR = 5.6 msec). The rabbits were injected with SPIO-3 (2 mmol Fe/kg) IV via an ear vein. Post-contrast MRI was performed on day 5 using the same MRI sequences. MRI was done with respiratory and cardiac gating. The rabbits were anesthetized with isoflurane for the duration of their studies.

Ex Vivo

All rabbits that underwent *in vivo* MRI were sacrificed. The aortas were excised, isolated, and placed in a gel medium. Both ends of the aorta were clamped and all side branches were occluded. Gadolinium-DTPA was injected inside the lumen. Then, MRI was performed, using the 1.5T scanner used in the *in vivo* experiments (Signa, General Electric). Data on T2 gradient echo and 3D MR angiography sequences were recorded for each specimen.

RESULTS

Intracellular Induction of Oxidative Stress

65

Lipid-coated SPIO-2 elicited significantly less NO production within macrophages than did dextran-coated SPIO-4. Also, as shown by studies using fluorescently labeled SPIO, the known mannose receptor inhibitor, mannan, significantly inhibited macrophage uptake of SPIO-4 but not SPIO-2.

Macrophage SPIO Uptake

In Vitro

The uptake of fluorescently labeled SPIO by macrophages was dose dependent. Three independent experiments yielded similar results.

In Vivo

Peritoneal macrophages readily took up fluorescently labeled SPIO. Circulating monocytes occasionally took up unlabeled SPIO.

Intracellular SPIO Relaxivity

A significant relationship was found between cellular SPIO incubation time and T2 shortening and between SPIO dose and T2 shortening ($P<0.05$). The maximum T2 shortening effect was observed to occur at echo time TE = 96 msec and repetition time TR = 3000 msec.

In Vivo SPIO Distribution in ApoE-Deficient vs. Wild-Type Mice

Histopathologic studies revealed the accumulation of SPIO particles in the monocyte/macrophage system in both normal and atherosclerotic mice, especially in the liver, spleen, and bone marrow. Other tissues, such as the lungs and kidneys also showed some degree of SPIO uptake, but mainly in the macrophage system. ApoE-deficient and wild-type normal mice differed in the extent of SPIO uptake by aortae and atherosclerotic lesions. Numerous iron particles were seen in aortic atherosclerotic plaques from ApoE-deficient mice, compared with very few in nonatherosclerotic areas of the aortic wall in both normal and ApoE-deficient mice.

In Vivo Distribution of SPIO in Rabbits

Histopathologic studies in rabbits also revealed the accumulation of iron in the monocyte/macrophage system in all tissues including the arterial wall . The correlation between iron accumulation and macrophage accumulation in the aortic wall was close ($r = 0.95$) and significant ($P<0.05$). Actively inflamed atherosclerotic areas of the aortic wall showed higher uptake of SPIO than did the normal aortic wall and noninflamed atherosclerotic areas.

Comparison of Pre- and Post-SPIO Contrast MRI

ApoE-Deficient vs. Normal Mice

MRI studies showed decreased signal intensity and irregularity in the aortic walls of SPIO-injected ApoE-deficient mice compared with no decrease in signal intensity and no irregularity in SPIO-injected C57BL wild-type (normal) mice. High-resolution images of the aortic wall were obtained at the level of the kidneys, aortic arch and root, and renal ostia in both ApoE-deficient and wild-type mice.

WHHL vs. NZW Rabbits

In Vivo

In vivo MRI studies revealed decreased signal intensity on 3D MR angiography in the aortic wall. Because SPIO uptake in the liver, spleen, bone marrow, and other tissues imposed a tissue artifact, changes in T1- and T2-weighted images of the aorta and other arteries could not be appreciated.

Ex Vivo

Ex vivo MRI studies were done to circumvent the tissue artifact mentioned above. As revealed by 3D MR angiography, there were significant luminal irregularities in the aortic walls of SPIO-injected WHHL mice. Also, as shown by T2*- weighted images of the SPIO-injected WHHL mice, SPIO had a negative enhancement effect in the intima and, to some extent, in the medial layer of the atherosclerotic aortic wall .

DISCUSSION

Herein, we are reporting for the first time that (1) lipid-coated SPIO is taken up by macrophages through a different pathway than dextran-coated SPIO, thus allowing more uptake of SPIO with potentially less oxidative stress; (2) activated monocytes avidly take up SPIO *in vitro*; (3) the T2 shortening effect of SPIO is preserved after SPIO uptake; (4) SPIO injected into ApoE-deficient mice accumulates in atherosclerotic plaques; (5) SPIO injected into hypercholesterolemic WHHL rabbits accumulates predominantly in superficial foamy cells in atherosclerotic cap; and (6) SPIO-enhanced MRI in atherosclerotic animals causing irregular darkening (signal loss) of the aortic wall indicating the presence of active inflammation (SPIO-loaded macrophages).

MRI is a major investigative tool in the field of cardiovascular disease and atherosclerosis, and its application to the visualization and structural characterization of atherosclerotic plaques has recently increased. Toussaint [21,22] Yuan,[7,23] Fayad,[8] and their colleagues have greatly contributed to this field by introducing high-resolution imaging of atherosclerotic plaques and developing methods for differentiating certain anatomic criteria of vulnerability (e.g., presence of a thin fibrous cap and neovascularization). However, no longitudinal study has correlated such findings with future cardiovascular or cerebrovascular events.

The use of SPIO as a MRI contrast agent for detecting atherosclerosis has been recently studied by Ruehm et al.[24] and Schmitz et al.[25,26] in hypercholesterolemic rabbits. Both groups observed a decrease in the signal intensity of aortic lesions after injecting SPIO. Ruehm et al.[24] observed this change on MR angiography of the aorta and also showed histologic evidence of SPIO in the atherosclerotic plaques, but they could not establish any correlations between

histopathology and MRI findings. However, because they did not use a SPIO-injected non-atherosclerotic control group in their experiments, it is unclear whether the observed changes in MRI were due to artifacts from SPIO particles in the surrounding tissues or to SPIO in the plaques. Using ultra-small SPIO, Schmitz et al.[25,26] observed changes in axial T2*-weighted images of the aortic wall. This group also did not report using a SPIO-injected non-atherosclerotic control. Neither of these two groups of investigators studied the interaction of monocytes/macrophages with SPIO *in vitro* or studied different types of SPIOs.

Our studies of SPIO uptake showed that macrophages in cell culture medium avidly take up SPIO and that the uptake of dextran-coated SPIO is dose dependent. This does not, however, seem to decrease macrophage viability. Our studies have shown that macrophages maintain their nuclear and cellular integrity.[27,28] Furthermore, we found that the amount of oxidative stress (an indicator of macrophage activity) induced by SPIO uptake varied by the type of SPIO. Using NO formation as an indicator of oxidative stress,[29] we noted that lipid-coated SPIO was associated with minimal NO formation and that its absorption appeared to occur mainly through scavenger receptors. Thus, lipid-coated SPIO may be an ideal plaque-targeted MRI contrast agent. In contrast, dextran-coated SPIO preferentially accumulated in the monocyte/macrophage system, and its absorption by macrophages appeared to be mediated at least in part by mannose receptors. Earlier investigations showed that dextran-coated SPIO particles were readily taken up by macrophages and tumor cell lines (e.g., C6) and suggested a possible role for opsonization in the uptake process[30]. Moreover, even though earlier experiments did not specify any potential candidate macrophage receptor for dextran-coated SPIO, they did identify at least one possible scavenger receptor for uptake of opsonized particles[31]. Consequently, dextran-coated SPIO might be more useful as a contrast agent for conventional MRI than as a contrast agent for MRI of lipid laden atherosclerotic plaques.

Our studies of MRI relaxivity revealed that intracellular SPIO retains its superparamagnetic properties to affect tissue relaxation time (especially T2). We also found that alteration in macrophage T2 relaxation changes with the intracellular concentration of SPIO, which itself correlates with the time of exposure to SPIO, this implies in turn that the T2 effect is enhanced at higher doses and longer incubation times.

In our studies in Apo E deficient mice, the atherosclerotic plaque burden and inflammation were more pronounced in the upper aorta. Moreover, we found that SPIO was unevenly distributed in the arterial tree. SPIO particles were more frequent in the aortic root than in distal aorta, relatively rare in the nonatherosclerotic wall, and unlike in the rabbit plaques, more often found near the center of plaques and in large foamy cells. Since ApoE-deficient mice do not have a well-developed fibrous cap, we could not locate SPIO particles within the caps of atherosclerotic plaques in these animals. This is in agreement with results of previous studies in ApoE-deficient mice showing fluorescently labeled macrophages within foam cell atherosclerotic plaques and adhering to the luminal surface of the plaques 48 hours after IV injection.[32] In addition, experiments aimed at quantifying monocyte/macrophage recruitment in atherosclerotic plaques in mice have shown that recruitment varies by stage of atherosclerosis in these plaques and also by location in the arterial tree.[33,34]

In our histopathologic studies of atherosclerotic plaques in

rabbits, SPIO accumulation was more pronounced in WHHL rabbits than in ApoE-deficient mice. However, areas of iron staining were more superficial in the rabbit plaques. Interestingly, SPIO particles were not evenly distributed in all plaques. Our initial observations indicate that areas with thick fibrous caps accumulate less SPIO while areas with minimal fibrosis and an abundance of subendothelial foamy cells accumulate more. Electron microscopy studies showed that almost all SPIO particles were intracellular. They also revealed sporadic localization in endothelial cells, though this may simply indicate diffusion into permeable areas of the endothelium.

In our MRI studies of the aorta, we found changes in both mice and rabbits after SPIO injection. In ApoE-deficient mice, we found irregularities and decreased signal intensity in T2*-weighted images of the aortic wall. In the rabbits, we found luminal irregularities in the aortic wall mainly in 3D MR angiographic images obtained with gadolinium-DTPA 5 days after SPIO injection. This effect was not observed in control animals. Because of their small size and problems with cardiac gating, we could not observe the thoracic aorta clearly enough to compare pre- and post-SPIO effects. Therefore, we focused on the changes in the abdominal aorta at the renal level. Also, in analyzing the T2*-weighted images of rabbits *in vivo*, we were unable to cancel out the noise caused by SPIO accumulation in the adjacent tissues (i.e., liver, spleen, lung, and bone marrow). Since similar irregularities in our control NZW rabbits suggested the possible deposition of iron artifacts in other tissues (i.e., spleen, liver, lung, and bone marrow), we decided to study the aortas of the atherosclerotic and normal rabbits *ex vivo*. This allowed us to more clearly visualize the aorta. It also revealed significant irregularities in the internal luminal side of the aorta that were not found in either SPIO-injected wild-type (non-atherosclerotic) rabbits or uninjected control WHHL rabbits.

CONCLUSIONS

SPIO-enhanced MRI was studied as a noninvasive means to detect macrophage infiltration in atherosclerotic plaques in the aortic walls of ApoE-deficient mice and WHHL rabbits. The injection of SPIO was not associated with any complications in these animals. Our findings suggest that SPIO-enhanced MRI may have significant potential for diagnosis of vulnerable plaques in a subset of vulnerable patients.

REFERENCES

1. Muller JE, Tofler GH, Stone PH. Circadian variation and triggers of onset of acute cardiovascular disease. *Circulation*. 1989;79:733-743.
2. Farb A, Tang AL, Burke AP, Sessums L, Liang Y, Virmani R. Sudden coronary death: frequency of active coronary lesions, inactive coronary lesions, and myocardial infarction. *Circulation*. 1995;92:1701-1709.
3. Libby P. What have we learned about the biology of atherosclerosis? The role of inflammation. *Am J Cardiol*. 2001;88:3J-6J.

4. Shah PK, Falk E, Badimon JJ, Fernandez-Ortiz A, Mailhac A, Villareal-Levy G, Fallon JT, Regnstrom J, Fuster V. Human monocyte-derived macrophages induce collagen breakdown in fibrous caps of atherosclerotic plaques. Potential role of matrix-degrading metalloproteinases and implications for plaque rupture. *Circulation*. 1995;92:1565-1569.

5. Libby P, Sukhova G, Lee RT, Galis ZS. Cytokines regulate vascular functions related to stability of the atherosclerotic plaque. *J Cardiovasc Pharmacol*. 1995;25(suppl 2):S9-S12.

6. Ambrose JA, Tannenbaum MA, Alexopoulos D, Hjemdahl-Monsen CE, Leavy J, Weiss M, Borrico S, Gorlin R, Fuster V. Angiographic progression of coronary artery disease and the development of myocardial infarction. *J Am Coll Cardiol*. 1988;12:56-62.

7. Yuan C, Petty C, O'Brien KD, Hatsukami TS, Eary JF, Brown BG. In vitro and in situ magnetic resonance imaging signal features of atherosclerotic plaque-associated lipids. *Arterioscler Thromb Vasc Biol*. 1997;17:1496-1503.

8. Fayad ZA, Fuster V, Fallon JT, Jayasundera T, Worthley SG, Helft G, Aguinaldo JG, Badimon JJ, Sharma SK. Noninvasive in vivo human coronary artery lumen and wall imaging using black-blood magnetic resonance imaging. *Circulation*. 2000;102:506-510.

9. Botnar RM, Stuber M, Kissinger KV, Kim WY, Spuentrup E, Manning WJ. Noninvasive coronary vessel wall and plaque imaging with magnetic resonance imaging. *Circulation*. 2000;102:2582-2587.

10. Velican C, Velican D. Atherosclerotic involvement of coronary branch vessels. *Atherosclerosis*. 1986;60:237-250.

11. Perdigao C, Andrade A, Monteiro J, Ribeiro C. [Coronary atherosclerosis in acute myocardial infarct. Anatomic profile of diverse causes of death]. *Rev Port Cardiol*. 1992;11:539-551.

12. De Franco AC, Nissen SE. Coronary intravascular ultrasound: implications for understanding the development and potential regression of atherosclerosis. *Am J Cardiol*. 2001;88:7M-20M.

13. Nissen S. Coronary angiography and intravascular ultrasound. *Am J Cardiol*. 2001;87:15-20.

14. Naghavi M, Madjid M, Khan MR, Mohammadi RM, Willerson JT, Casscells SW. New developments in the detection of vulnerable plaque. *Curr Atheroscler Rep*. 2001;3:125-135.

15. Slager CJ, Wentzel JJ, Schuurbiers JC, Oomen JA, Kloet J, Krams R, von Birgelen C, van der Giessen WJ, Serruys PW, de Feyter PJ. True 3-dimensional reconstruction of coronary arteries in patients by fusion of angiography and IVUS (ANGUS) and its quantitative validation. *Circulation*. 2000;102:511-516.

16. Silber HA, Bluemke DA, Ouyang P, Du YP, Post WS, Lima JA. The relationship between vascular wall shear stress and flow-mediated dilation: endothelial function assessed by phase-contrast magnetic resonance angiography. *J Am Coll Cardiol*. 2001;38:1859-1865.

17. Kanno S, Lee PC, Dodd SJ, Williams M, Griffith BP, Ho C. A novel approach with magnetic resonance imaging used for the detection of lung allograft rejection. *J Thorac Cardiovasc Surg*. 2000;120:923-934.

18. Kanno S, Wu YJ, Lee PC, Dodd SJ, Williams M, Griffith BP, Ho C. Macrophage accumulation associated with rat cardiac allograft rejection detected by magnetic resonance imaging with ultrasmall superparamagnetic iron oxide particles. *Circulation*. 2001;104:934-938.

19. Dousset V, Ballarino L, Delalande C, Coussemacq M, Canioni P,

Petry KG, Caille JM. Comparison of ultrasmall particles of iron oxide (USPIO)-enhanced T2-weighted, conventional T2-weighted, and gadolinium-enhanced T1-weighted MR images in rats with experimental autoimmune encephalomyelitis. *AJNR Am J Neuroradiol.* 1999;20:223-227.

20. Pouliquen D, Le Jeune JJ, Perdrisot R, Ermias A, Jallet P. Iron oxide nanoparticles for use as an MRI contrast agent: pharmacokinetics and metabolism. *Magn Reson Imaging.* 1991;9:275-283.

21.   Toussaint JF, LaMuraglia GM, Southern JF, Fuster V, Kantor HL

Magnetic resonance images lipid, fibrous, calcified, hemorrhagic, and

thrombotic components of human atherosclerosis in vivo. *Circulation.*

1996 ;94:932-938.

22.   Toussaint JF, Southern JF, Kantor HL, Jang IK, Fuster V.

Behavior of atherosclerotic plaque components after in vitro

angioplasty and atherectomy studied by high field MR imaging. *Magn*

Reson Imaging 1998;16:175-183

23. Yuan C, Zhang SX, Polissar NL, Echelard D, Ortiz G, Davis JW, Ellington E, Ferguson MS, Hatsukami TS. Identification of fibrous cap rupture with magnetic resonance imaging is highly associated with recent transient ischemic attack or stroke. *Circulation.* 2002;105:181-185.

24. Ruehm SG, Corot C, Vogt P, Kolb S, Debatin JF. Magnetic resonance imaging of atherosclerotic plaque with ultrasmall superparamagnetic particles of iron oxide in hyperlipidemic rabbits. *Circulation.* 2001;103:415-422.

25. Schmitz SA, Winterhalter S, Schiffler S, Gust R, Wagner S, Kresse M, Coupland SE, Semmler W, Wolf KJ. USPIO-enhanced direct MR imaging of thrombus: preclinical evaluation in rabbits. *Radiology.* 2001;221:237-243.

26. Schmitz SA, Taupitz M, Wagner S, Wolf KJ, Beyersdorff D, Hamm B. Magnetic resonance imaging of atherosclerotic plaques using superparamagnetic iron oxide particles. *J Magn Reson Imaging.* 2001;14:355-361.

27. Chateau MT, Caravano R. Rapid fluorometric measurement of the intra-cellular concentration of ciprofloxacin in mouse peritoneal macrophages. *J Antimicrob Chemother.* 1993;31:281-287.

28. Sarih M, Souvannavong V, Brown SC, Adam A. Silica induces apoptosis in macrophages and the release of interleukin-1 alpha and interleukin-1 beta. *J Leukoc Biol.* 1993;54:407-413.

29. Forman HJ, Torres M. Redox signaling in macrophages. *Mol Aspects Med.* 2001;22:189-216.

30. Schulze E, Ferrucci JT Jr, Poss K, Lapointe L, Bogdanova A, Weissleder R. Cellular uptake and trafficking of a prototypical magnetic iron oxide label in vitro. *Invest Radiol.* 1995;30:604-610.

31. Moore A, Weissleder R, Bogdanov A Jr. Uptake of dextran-coated monocrystalline iron oxides in tumor cells and macrophages. *J*

Magn Reson Imaging. 1997;7:1140-1145.

32.   Patel SS, Thiagarajan R, Willerson JT, Yeh ET. Inhibition of alpha4 integrin and ICAM-1 markedly attenuate macrophage homing to atherosclerotic plaques in ApoE-deficient mice. *Circulation*. 1998;97:75-81.

33.   Steinberg D, Khoo JC, Glass CK, Palinski W, Almazan F. A new approach to determining the rates of recruitment of circulating leukocytes into tissues: application to the measurement of leukocyte recruitment into atherosclerotic lesions. *Proc Natl Acad Sci U S A*. 1997;94:4040-4044.

34.   Kim CJ, Khoo JC, Gillotte-Taylor K, Li A, Palinski W, Glass CK, Steinberg D. Polymerase chain reaction-based method for quantifying recruitment of monocytes to mouse atherosclerotic lesions in vivo: enhancement by tumor necrosis factor-_ and interleukin-1_. *Arterioscler Thromb Vasc Biol*. 2000;20:1976-1982.

Project II.G. "Gene Transfer of Tissue Factor Pathway Inhibitor (TFPI)"

Investigator: Pierre Zoldhelyi, M.D.

The progress we have made with regard to the work outlined in the DREAMS proposal IIG has allowed us to conclude that gene transfer of TFPI to injured arteries protect the injured vessels against thrombosis and internal scarring, which gradually obtructs the vessel lumen and interrupts vital blood flow. These findings have been published in peer-reviewed journals, includig Circulation and the Proceedings of the Academy of Sciences USA. They have resulted in issuance of a US patent of TFPI vascular gene therapy.

BACKGROUND

Tissue factor, a transmembrane protein receptor, is the cellular initiator of thrombin generation and blood coagulation in hemostasis and thrombosis. After its exposure following vessel injury or cytokine activation, tissue factor binds to circulating factor VIIa and, in the extrinsic pathway of blood coagulation, activates factor X, which in the prothrombinase complex converts prothrombin to thrombin.

Tissue factor- driven thrombin generation plays a pivotal role in thrombosis, possibly in restenosis after percutaneous revascularization, and contributes to the thrombogenicity of the atherosclerotic plaque. Recently, recombinant tissue factor pathway inhibitor (rTFPI) has been studied in animal models as an approach to the prevention of thrombosis and restenosis after arterial injury. At physiological concentrations, TFPI binds to factor Xa, and this complex associates with and inhibits tissue factor/factor VIIa. Higher concentrations of TFPI can inhibit tissue factor/factor VIIa in the absence of factor Xa.

Although attractive in principle, it is uncertain whether short-term administration of rTFPI will achieve lasting vasoprotection after percutaneous revascularization, particularly at sites doses of recombinant TFPI capable of preventing arterial thrombosis and potentially restenosis are substantial (100 mg/kg/min) and may entail significant hemorrhagic risks. Here, we investigated in a porcine model whether local gene transfer of human TFPI can prevent platelet-driven thrombosis and flow reduction at sites of severe carotid injury and increased shear stress and whether antithrombotic protection would occur without systemic hemostatic impairment.

EFFECT OF TFPI GENE TRANSFER IN A PORCINE ANGIOPLASTY INJURY MODEL: *Effects of TFPI gene transfer on thrombus formation.*

Balloon-injured porcine carotid arteries were treated locally with an adenovirus encoding human TFPI (Ad-TFPI) or control virus. Gene

transfer of TFPI was confirmed by detection of human TFPI in the conditioned medium of porcine carotid arteries kept in culture after in vivo transduction. When carotid flow was measured with Doppler probe 5 days after surgery, cyclic flow variations (CFVs) developed in 7 of 8 control pigs after constriction of the injured carotid artery by 40%, and all control-treated arteries occluded after 70% constriction. In contrast, CFVs were observed in only 1 of 8 Ad-TFPI-treated pigs after 40% constriction, and only 3 of 8 occluded after constriction by 70% (P50.0027 and P50.007, respectively). None of the 5 TFPI-transduced arteries open after 70% constriction developed CFVs during an incremental epinephrine infusion. **Conclusions**—Compared with baseline, systemic hemostatic variables and platelet aggregation were unimpaired, suggesting that TFPI gene transfer can prevent arterial thrombosis in the presence of severe shear stress and without detectable hemostatic impairment. (Circulation. 2000;101:289-295.)

LOCAL GENE TRANSFER OF TISSUE FACTOR PATHWAY INHIBITOR

REGULATES INTIMAL HYPERPLASIA IN ATHEROSCLEROTIC ARTERIES

Tissue factor (TF), the initiator of blood coagulation and thrombosis, is up-regulated after vascular injury and in atherosclerotic states. Systemic administration of recombinant TF pathway inhibitor (TFPI) has been reported to decrease intimal hyperplasia after

vascular injury and also to suppress systemic mechanisms of blood coagulation and thrombosis. In heritable hyperlipidemic Watanabe rabbits, adenoviral gene transfer of TFPI to balloon-injured atherosclerotic arteries reduced the extent of intimal hyperplasia by 43% ($P < 0.05$) compared with a control vector used at identical titer (1 and 3 10e10 plaque-forming units/ml). Platelet aggregation and coagulation studies performed 7 days

after local gene transfer of TFPI failed to show any impairment in systemic hemostasis. At time of sacrifice, 4 weeks after vascular injury, the 10 Ad-TFPI treated carotid arteries were free of thrombi, whereas two control-treated arteries were occluded (P, not significant). These findings suggest that TFPI overexpressed in atherosclerotic arteries can regulate hyperplastic response to injury in the absence of changes in the hemostatic system, establishing a role for local TF regulation as target for gene transfer-based antirestenosis therapies.

More recently, we extended these observations to mechanically damaged *atherosclerotic* arteries and *vein grafts*, where we found that adenoviral cyclooxygenase-1 (PGHS-1) gene transfer to damaged carotid

arteries and vein grafts of hypercholesterolemic rabbits did not reduce intimal hyperplasia but nonetheless resulted in preservation of (normal) blood flow velocity due to marked dilatation of the vessels 1 month after surgery. *Combining PGHS-1 with TFPI gene transfer* resulted in reduction of intimal hyperplasia, suppressed thrombosis, and allowed a 50% reduction of the viral load (titer in pfu/ml), without loss of efficacy.

The efficacy of antithrombotic adenoviral gene therapy with the TFPI and PGHS-1 genes to atherosclerotic arteries can be schematically summarized by the cartoon shown in Figure 1.
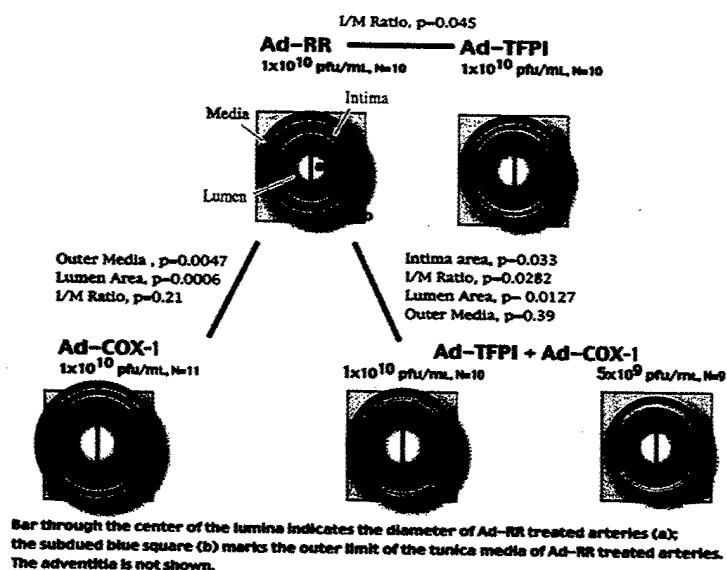

I/M Ratio, p=0.045

Ad-RR ———— **Ad-TFPI**
1x10^{10} pfu/mL, N=10   1x10^{10} pfu/mL, N=10

Intima
Media
Lumen

Outer Media , p=0.0047   Intima area, p=0.033
Lumen Area, p=0.0006   I/M Ratio, p=0.0282
I/M Ratio, p=0.21   Lumen Area, p= 0.0127
                            Outer Media, p=0.39

Ad-COX-1   **Ad-TFPI + Ad-COX-1**
1x10^{10} pfu/mL, N=11   1x10^{10} pfu/mL, N=10   5x10^9 pfu/mL, N=9

Bar through the center of the lumina indicates the diameter of Ad-RR treated arteries (a); the subdued blue square (b) marks the outer limit of the tunica media of Ad-RR treated arteries. The adventitia is not shown.

Figure 1. Cartoon outlining the structural changes of balloon-injured carotid arteries of Watanabe rabbits, as observed on postmortem histological examination 4 weeks after surgery. All animals were pressure perfusion-fixed at the time of sacrifice in order to maintain original (in vivo) vascular dimensions.

We have now begun to develop new , long-term expressing gene vectors associated with no known toxicity or inflammation. These "adenovirus-associated virus" vectors are most promising and the testing of these will represent a new milestone in our resarch related to this project (DREAMS IIG).

REFERENCES RELATED TO THE WORK IN DREAMS 2G

Zoldhelyi P., Chen Z., McNatt J.M., Eichstaedt H.C., Willerson J.T.: Combined gene transfer of cyclooxygenase and tissue factor pathway inhibitor markedly reduces neointima formation and stenosis and

improves lumen area in balloon-injured atherosclerotic arteries. *Circulation 2001;* 104 (Suppl. II):II-17.

Eichstaedt H.C., Nolden L.N., Shelat H.S., Willerson J.T., **Zoldhelyi P.**: Adenoviral gene transfer of cyclooxygenase enhances prostacyclin synthesis in vascular smooth muscle cells and markedly improves lumen size in atherosclerotic vein grafts. *Circulation 2001;* 104 (Suppl. II):II-31

Eichstaedt, H.C., Daniel S.S., Nolden L.K., Shelat H.S., Willerson J.T., **Zoldhelyi P.**: Adenoviral gene transfer of cyclooxygenase-1 enhances prostacyclin synthesis in vascular smooth muscle cells and markedly improves lumen size in atherosclerotic vein grafts. *Circulation 2001;* 102(Suppl.II):II-190.

Zoldhelyi, P., Chen, Z.-Q., Shelat H.S., McNatt, J.M., Willerson, J.T.: Gene transfer of tissue factor pathway inhibitor regulates intimal hyperplasia in atherosclerotic arteries. *Proc. Natl. Acad. Sci. U.S.A. 2001;* 98:4078-4083.
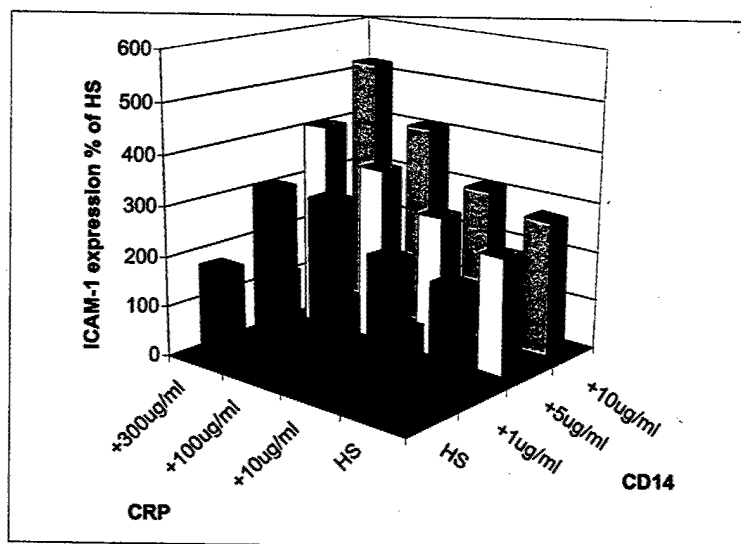
Project III.A. "Induction of Chemokine Expression in Endothelial Cells by C-Reactive Protein"

Investigator: Edward T.H. Yeh, M.D.

Introduction: Inflammation is now known to be a major player in the development of atherosclerosis and its subsequent events, such as acute coronary syndrome [1]. C-Reactive Protein (CRP) has been shown to be an excellent marker of inflammation that also predicts the risk of heart attack in apparently healthy men and women. We have shown that CRP can directly activate human coronary endothelial cells [2], [3].. Thus, CRP is not only a marker, but also a culprit in setting up a chain of events that eventually leads to heart attack. Another important inflammatory marker is CD14, which is an acute phase protein that binds to lipopolysachrides (LPS) and is critically involved in LPS-mediated activation of endothelial cells. However, the role of CD14 and LPS in the pathogenesis of acute coronary syndrome has not been clearly elucidated. We hypothesized that CRP, one of the strongest predictors of future cardiovascular events, may synergize with CD14 and LPS in activation of arterial endothelium and this mechanism may be important in acute coronary syndromes.

Research accomplishments:

In order to show the synergy of CRP and CD14, cultured human umbilical vein endothelial cells were cultured with variable doses of CRP and CD14 in the presence of "physiological" concentrations of LPS. As shown in the figure, CRP synergize with CD14 in the presence of LPS to induce ICAM-1 expression in endothelial cells. At the highest dose of CRP and CD14, there is a 5-fold increase in the expression of ICAM-1.

Conclusion: These results further strengthen the role of CRP in the pathogenesis of vascular inflammation and, likely, atherosclerosis. Furthermore, CD14 and CRP are not merely biological markers of inflammation, but can synergize with each other in the activation of endothelial cells.

References:

1. Pasceri V, Yeh ET. A tale of two diseases: atherosclerosis and rheumatoid arthritis. *Circulation*. 1999;100:2124-6.
2. Pasceri V, Willerson JT, Yeh ET. Direct proinflammatory effect of C-reactive protein on human endothelial cells. *Circulation*. 2000;102:2165-8.
3. Pasceri V, Chang J, Willerson JT, Yeh ET. Modulation of c-reactive protein-mediated monocyte chemoattractant protein-1

induction in human endothelial cells by anti-atherosclerosis drugs. *Circulation*. 2001;103:2531-4.

Project III.B. "Nitrotyrosine formation, metabolism and function"

Investigator: Ferid Murad, M.D., Ph.D.

INTRODUCTION

The biological effects of nitric oxide may be due to increased cyclic GMP synthesis by guanylyl cyclase or by cyclic GMP-independent pathways. With regard to the latter, one of the important effects of nitric oxide is the interaction with superoxide anion to form peroxynitrite. Peroxynitrite is very reactive and can modify proteins, DNA and lipids. One of its effects is to form nitrotyrosine with tyrosine residues in proteins or with free tyrosine. Our laboratory is examining the proteins that may contain nitrotyrosine in order to identify these proteins and determine their function. We are also characterizing an enzyme activity that we call a "denitrase" that can modify nitrotyrosine residues in proteins.

PROGRESS & RESULTS

In order to induce inflammatory processes and increase peroxynitrite and nitrotyrosine formation we have administered LPS (endotoxin) or proinflammatory cytokines such as IFN-_, IL-1, or TNF-_ to cell cultures or intact animals (rats). We have also induced diabetes in rats with the administration of streptozotocin, a well-known model to produce diabetes. Another model of gastrointestinal inflammation has been the oral administration to rats and mice of the parasite, Trichinella spiralis.

Tissue samples are homogenized and fractions are applied to 1-D and/or 2-D PAGE for the separation of proteins. Nitrated proteins are further identified by matrix-assisted laser desorption ionization/time-of-flight mass spectrometric analysis (MALDI-TOF) of in-gel tryptic digest of nitrotyrosine immunopositive bands. We use commercial nitrotyrosine antibodies and those that we have prepared for nitrotyrosine immunohistochemistry and/or Western immunoblots. Tissue sections have also been examined by immunohistochemical techniques for nitrotyrosine.

With LPS administration to rats at 10 mg/kg for various times (1 to 24 hours) a number of proteins in various tissues including several proteins in kidney and heart became nitrated. One of the nitrotyrosine-containing proteins in kidney and heart has been identified as succinyl-CoA-oxyacid-CoA Transferase (SCOT). This enzyme is a mitochondrial enzyme that converts ketone bodies to acetyl CoA for metabolism in the Krebs cycle. Nitration is induced by either LPS or streptozotocin administration and the enzyme's activity is decreased. A manuscript was submitted describing these studies (13).

We have also found that diabetes results in the nitration of cyclic GMP-dependent protein kinase in vascular tissue. The nitration is associated with altered cyclic GMP activation of the enzyme requiring higher concentrations of cyclic GMP.

Three nitrotyrosine-containing proteins have also been identified in human platelets that are aggregated with thrombin treatment.

These proteins are cytoskeletal proteins. In rat lung tissue a selenium binding protein and ERK-2 have been found to be nitrated. The function of the selenium binding protein is unknown, while ERK-2 participates in MAP kinase activation and cell proliferation. In small intestine several nitrated proteins have been found after LPS administration or Trichinella infection. These proteins have yet to be sequenced and identified.

Clearly a number of proteins can be nitrated on tyrosine residues with LPS administration, infection with Trichinella, or diabetes. Some of these proteins are enzymes that serve in important metabolic pathways or cellular signaling pathways.

Apart from biological significance of protein nitration, the mechanism(s) of tyrosine nitration in vivo is also a subject of our interest. Tyrosine nitration is a free radical-mediated process, and the understanding of formation of nitrating agents in vivo is of great importance for the evaluation and design of antioxidant therapy in different inflammatory conditions. In addition to peroxynitrite-dependent nitration, other reactions, for example those involving nitrate and peroxidases, may give a rise to protein nitration. We have compared the 2-D-PAGE patterns of tyrosine nitrated proteins generated in different in vitro conditions with those found in specific in vivo conditions. Our studies show that protein nitration could be the biochemical marker for inflammation development, and suggest that the same primary nitrating agent is formed through different nitrating pathways (paper submitted - reference 21).

We have also obtained some evidence that nitrotyrosine in proteins can be modified by an enzyme in tissues that we have called "denitrase". This enzyme modifies the nitrotyrosine epitope but the product of the reaction is presently unknown (12). Protein nitration may be a reversible reaction that participates in cellular regulation and signaling.

CONCULSIONS

Clearly some proteins can be nitrated in their tyrosine residues. This may alter their activity and may be a reversible process. These results support the view that protein (tyrosine) nitration may be an important physiological process that participates in cellular regulation and cellular signaling.

PUBLICATIONS DURING THE DREAMS SUPPORT

(1)   Martin, E., Davis, K., Bian, K., Lee, Y.C., and Murad, F.
       Cellular signaling with NO and cyclic GMP. **Seminars in Perinatology** 24, 2-6, 2000.

(2)   Ishii, N., Patel, K.P., Lane, P.H., Taylor, T., Bian, K., Murad, F., Pollock, J.S., and Carmines, P.K. Nitric oxide synthesis and oxidative stress in the renal cortex of rats with diabetes mellitus. **J. Amer. Soc. Nephrology** 12, 1630-1639, 2001.

(3) Mendes, R.V., Martins, A.R., de Nucci, G., Murad, F., and Soares, F.A. Expression of nitric oxide synthase isoforms and nitrotyrosine immunoreactivity by B-cell non-Hodgkin's lymphomas and multiple myeloma. **Histopathology** 39, 172-178, 2001.

(4) Bian, K., Harari, Y., Zhong, M., Lai, M., Castro, G., Weisbrodt, N., and Murad, F. Down regulation of inducible nitric oxide synthase during parasite-induced gut inflammation. A path to identify a selective NOS-2 inhibitor. **Molecular Pharmacology** 59, 939-947, 2001.

(5) Sharina, I., Krumenacker, J., Martin, E., and Murad, F. Genomic organization of alpha$_1$ and beta$_1$ subunits of mammalian soluble guanylyl cyclase genes. **Proc. Nat. Acad. Sci.** 97, 10878-10883, 2000.

(6) Lee, Y.C., Martin, E. and Murad, F. Human recombinant soluble guanylyl cyclase: Expression, purification, and regulation. **Proc. Nat. Acad. Sci.** 97, 10763-10768, 2000.

(7) Krumenacker, J., Hyder, S. and Murad, F. Estradiol rapidly inhibits soluble guanylyl cyclase expression in rat uterus. **Proc. Nat. Acad. Sci.** 98, 717-722, 2001.

(8) Chen, Z.J., Miao, Z.H., Chang, G.D., Hughes, B., Vetter, M., Dulin, N., Murad, F., Douglas, J. and Chang, C.H. Molecular cloning of a regulatory protein for membrane-bound guanylyl cyclase GCA (submitted).

(9) Kildsgaard, J., Hollmann, T., Matthews, K., Bian, K., Murad, F. and Wetsel, R. Increased susceptability to endotoxin shock in complement C3a receptor deficient mice indicates an anti-inflammatory role for the C3a anaphylatoxin. **Journal of Immunology.** 165, 5406-5409, 2000.

(10) Murad, F. Discovery of some of the biological effects of nitric oxide and its role in cell signaling. Science and technology development: A retrospective view over the past century and a perspective look into the future. pp. 86-96. Editor in Chief: Lu, Yongxiang, ShangHai Education Press, ShangHai, 2000.

(11) Mailman, D., Guntuku, S., Bhuiyan, B. and Murad, F. Sites of LPS-induced nitric oxide production in the anesthetized rat. **Nitric Oxide: Biology and Chemistry** 5, 243-251, 2001.

(12) Davis, K., Martin, E., Turko, I. and Murad, F. Novel effects of nitric oxide, Annual Review of Pharmacology and Toxicology. 41, pp. 203-236, 2001.

(13) Marcondes, S., Turko, I., and Murad, F. Nitration of succinyl Co-A-axoacid transferase decreases enzyme activity with endotoxin administration. **Proc. Nat. Acad. Sci.** 98, 7146-7151, 2001.

(14) Seminara, A.R., Krumenacker, J.S., and Murad, F. Signal transduction with nitric oxide, guanylyl cyclase and cyclic GMP. In Proc. of the NATO meeting on Nitric Oxide, Sicily, NATO Science Series 317, 5-22, 2001.

81

(15) Hanafy, K., Krumenacker, J. and Murad, F. Nitric oxide and cyclic GMP cellular signaling. Proceedings of the Vascular Biology Conference, Cracow, Poland, Medical Science Monitor 7 (4), 801-819, 2001.

(16) Turko, I., Marcondes, S., and Murad, F. Diabetes-associated nitration of tyrosine and inactivation of succinyl-CoA:3-oxoacid CoA transferase. **Physiol. Amer. J. Physiol., Heart Circ** 281, H2289-H2294, 2001.

(17) Martin, E., Lee, Y.C., and Murad, F. YC-1 activation of human soluble guanylyl cyclase has both heme-dependent and heme—independent components. **Proc. Nat. Acad. Sci.** 98, 12938-12942, 2001.

(18) Bian, K., Zhong, M., Harari, Y., Weisbrodt, N., and Murad, F. Down regulation of inducible nitric oxide synthase by an IL4R_/Stat6-dependent and T-cell independent pathway during parasite-induced gut inflammation. **Mol Pharmacol.** 59(4):939-47, 2001.

(19) Bian, K., and Murad, F. Diversity of endotoxin-induced nitrotyrosine formation in macrophage – endothelium rich tissue. **Free Radical Biology and Medicine** 31(4):421-429, 2001.

(20) Turko, I., and Murad, F. Protein nitration in cardiovascular diseases. **Pharmacological Reviews** (In press).

(21) Turko, I., Aulak, K.S., Stuehr, D.J., and Murad, F. Protection of mitochondrial proteins from nitration. (Submitted).

(22) Adewuya, O., Irie, Y., Bian, K., Onigu-Otite, E., and Murad, F. Mechanism of vasculitis and aneurysms in a mouse model of Kawasaki Diseased: Role of nitric oxide. **Nitric Oxide: Biology and Chemistry**. (In press).

Project III.C. "Genes regulating wound healing and susceptibility to oxidative injury"

Investigators: Yong-Jian Geng, M.D., Ph.D. and James T. Willerson, M.D.

Hypothesis

We hypothesize that apolipoprotein-E deficiency induces broad alterations in expression of genes coding for proteins with various functions, such as cell structuring, adhesion, enzymatic reaction and apoptosis-regulation. Our goal is to employ the cDNA array technique to examine expression of genes involved in oncogenes, tumor suppressors, cell cycle regulators, stress proteins, ion channels/transports, receptors for cytokines/growth factors and hormones, adhesion proteins, regulators of apoptosis and DNA synthesis/repair, cytoskeletal proteins and proteases in the aortic tissues of apoE-null mice.

Technical Objectives and Methods

We employed a newly developed cDNA array technique to simultaneously analyze expression of hundreds of genes in the arterial tissue of apoE and wild type mice. Total RNA was isolated using a RNA isolation kit from Clontech (Palo Alto, CA). The cDNA arrays and hybridization were carried out using an AtlasTM cDNA Expression Arrays System (Clontech) with two identical nylon membranes arrayed with nearly 600 cDNA clones as listed in the user manual. The arrayed clones contain the genes encoding 6 groups of proteins involved in a broad range of cellular functions and metabolisms in addition to a group of "house-keeping" control proteins. The Atlas Arrays membranes were pre-heated at 68°C and then incubated with the radioactive cDNA probes synthesized from poly A^+ RNA in a hybridization solution containing 0.5% SDS overnight. The membranes were washed in 2 X SSC and 1% SDS at 68°C, and then exposed to Kodak BioMax MS X-ray film at -70°C. The radiographs of the probed membranes were scanned, and intensity of the hybridization was measured and analyzed with the software Atlasimage (Clontech).

Preliminary Results

It is known that age serves as a major risk factor for atherogenesis. We therefore examined whether the aortas of younger apoE-null mice showed a different pattern of gene expression than that in older apoE-null mice. In order to increase the clarity of the hybridization, a light exposure time was adapted to develop the radiographs. This led to development of a better image of the hybridization (Fig.1), while the background noise declined. The overall pattern of expression of the group C genes by the younger apoE-null mice was similar to the wild type controls at 3 months of age. We focused on the group C and group F genes, as the two groups showed most active patterns of hybridization. In group C, we clearly observed an increase in expression of certain genes, including apolipoprotein-J or clusterin, and the DNA double strand break repair protein PW-29, in the aortas of 15 months old apoE-null mice with advancing atherosclerosis (Fig. 1). The gene coding for glutathione peroxidase (selenoprotein) was found abundantly in the aortas of both wild type and apoE-null mice (Fig. 1). However, older apoE-null mice appeared to express higher levels of this gene, compared to wild type and younger (3 months) apoE-null mice. We detected similar patterns of gene expression in group F. For instance, we found that there was increased expression of the genes coding for the DNA excision repair protein ERCC-1, and the G/T-mismatch binding protein GTBP. Thus, alterations in gene expression in the aorta appeared to be age- and/or advancing atherosclerosis-dependent in apoE-null mice.
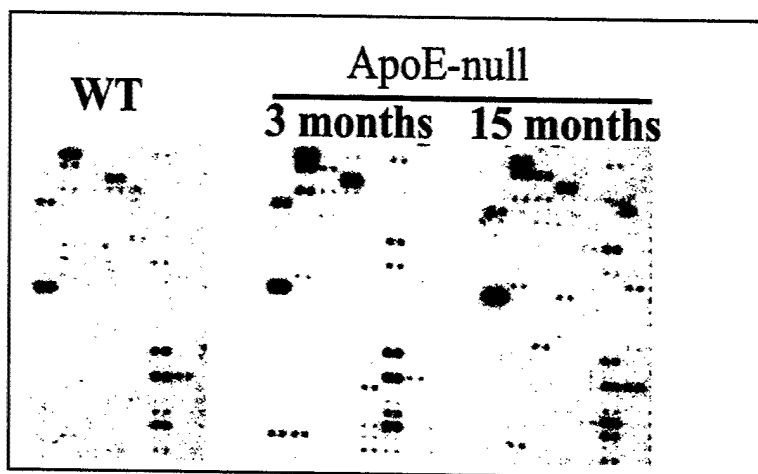
Fig. 1 cDNA arrays of mRNA isolated from the aortas of wild type (WT) and apolipoprotein-E-null (apoE-null) mice. Dots indicate arrayed cDNA hybridized with ^{32}P-labeled probes synthesized from mRNA.

In order to characterize expression of certain genes that encode proteins with different functions and biological activities, we performed the trend analysis by linear regression after dividing the genes tested into different subgroups. The results from this study show consistently that the pattern of gene expression in the aortas of apoE-null mice differs from that in wild type mice. We observed that expression of numerous genes in the aortas with atherosclerosis occurred at levels different from that in the wild type controls, pointing to a complex process of gene regulation and expression during the development of atherosclerosis. However, there were few changes in expression of the genes coding for the well-characterized "house-keeping" controls, such as ubiquitin, G3PDH, and b-actin. The specificity for the differential hybridization is further demonstrated by the fact that there was no hybridization toward negative control genes from microorganisms. Although an alteration in gene expression is not unexpected in the atherosclerotic arteries, it is surprising that there is such a broad variation in expression in certain groups of genes, in particular those involved in apoptosis, DNA repair, cell-cell communication and protein turnover. Expression of genes involved in inflammation such as proinflammatory cytokines, adhesion proteins, transcription factors and platelet activation occur in apoE-null mice clearly reflects the fact that atherosclerotic lesions contain numerous inflammatory mediators and cells. Genes that regulate apoptosis are up-regulated suggesting that expression of endogenous death-regulating genes contribute to regulation of cellularity in the atherosclerotic vessel wall. On the other hand, we observed almost equal numbers of other genes that were down-regulated, including cytokeratin, heat shock protein-27, p53 and protooncogenes (Pim-1, Ski, Cot, and B-Raf). Those changes provide evidence that an imbalance between vascular injury and repair may have taken place in the murine aorta with the development of atherosclerosis. Recent studies have suggested that during atherogenesis, vascular cell survival and death may be deregulated, leading to a broad spectrum of pathological alterations, including remodeling, lipid-core formation and plaque rupture. Altered expression of genes involved in apoptosis, a form of genetically programmed cell death, may therefore have an impact on the progression of atherosclerotic lesions. It is known that atherogenesis is a long-lasting, age-dependent process with complicated interactions between environmental factors and cells in the vessel wall, leading to the development of atherosclerotic plaques. Early studies have shown that atherosclerotic lesions develop primarily in the aortic roots of apoE-null mice. However,

with aging, the lesions expand to other parts of aortas such as the descending aortas. Although there were no major atherosclerotic lesions found in the descending aortas of younger mice (3 month old), altered gene expression was ready detectable. Interestingly, the increased gene expression in the younger mice was frequently seen in the genes coding for apolipoprotein-J or clusterin and DNA-binding protein.

Plan for further investigation

Our further studies will focus on individual gene expression and protein profiles in these animal models. We will characterize the molecular mechanisms underlying the altered gene expression during the development of atherosclerosis and wound healing. In addition, we will address whether function and metabolism of the blood vessel wall has been damaged during atherogenesis. Immunoblotting and 2D gel/Mass analysis will be conducted to determine the protein levels and sequence.

References

1. Ross R: Atherosclerosis--an inflammatory disease. N Engl J Med. 1999; 340:115-126.
2. Ross R: Cell biology of atherosclerosis. Annu Rev Physiol. 1995; 57:791-804.
3. DeRisi J, Penland L, Brown PO, Bittner ML, Meltzer PS, Ray M, Chen Y, Su YA, Trent JM: Use of a cDNA microarray to analyse gene expression patterns in human cancer. Nat Genet. 1996; 14:457-460.
4. DeRisi JL, Iyer VR: Genomics and array technology. Curr Opin Oncol. 1999; 11:76-79.
5. Adams MD, Kerlavage AR, Fields C, Venter JC: 3,400 new expressed sequence tags identify diversity of transcripts in human brain. Nat Genet. 1993; 4:256-267.
6. Heller RA, Schena M, Chai A, Shalon D, Bedilion T, Gilmore J, Woolley DE, Davis RW: Discovery and analysis of inflammatory disease-related genes using cDNA microarrays. Proc Natl Acad Sci U S A. 1997; 94:2150-2155.
7. Rubin EM, Smith DJ: Atherosclerosis in mice: getting to the heart of a polygenic disorder. Trends Genet. 1994; 10:199-203.
8. Smith JD: Mouse models of atherosclerosis. Lab Anim Sci. 1998; 48:573-579.
9. Plump AS, Smith JD, Hayek T, Aalto-Setala K, Walsh A, Verstuyft JG, Rubin EM, Breslow JL: Severe hypercholesterolemia and atherosclerosis in apolipoprotein E-deficient mice created by homologous recombination in ES cells. Cell. 1992; 71:343-353.
10. Smith JD, Breslow JL: The emergence of mouse models of atherosclerosis and their relevance to clinical research. J Intern Med. 1997; 242:99-109.